

# Inclusive Pion Double Charge Exchange in $^4\text{He}$ at Intermediate Energies

E. R. Kinney\* and J. L. Matthews

*Department of Physics and Laboratory for Nuclear Science  
Massachusetts Institute of Technology, Cambridge, Massachusetts 02139*

P. A. M. Gram,<sup>†</sup> D. W. MacArthur, and E. Piasetzky<sup>‡</sup>

*Los Alamos National Laboratory, Los Alamos, New Mexico 87545*

G. A. Rebka, Jr. and D. A. Roberts<sup>§</sup>

*Department of Physics, University of Wyoming, Laramie, Wyoming 82071*

(Dated: November 6, 2018)

## Abstract

A systematic experimental study of inclusive pion double charge exchange in  ${}^4\text{He}$  has been undertaken. The reaction  ${}^4\text{He}(\pi^+, \pi^-)4p$  was observed at incident energies 120, 150, 180, 240 and 270 MeV; the  ${}^4\text{He}(\pi^-, \pi^+)4n$  reaction was observed at incident energies 180 and 240 MeV. At each incident energy, the doubly differential cross section was measured at three to five outgoing pion laboratory angles between  $25^\circ$  and  $130^\circ$ . At each angle, cross sections were measured over the range of outgoing pion energies from 10 MeV up to the kinematic limit for the reaction in which the final state consists of the oppositely charged pion plus four free nucleons.

The spectra of outgoing pions are strikingly different from those observed for the inclusive double charge exchange reaction in heavier nuclei, but resemble those observed in the  $(\pi^-, \pi^+)$  reaction in  ${}^3\text{He}$ . The forward-angle spectra in the  ${}^3\text{He}$  and  ${}^4\text{He}$  reactions exhibit a prominent peak at high outgoing pion energies. Interpretation of the peaks in  ${}^3\text{He}$  ( ${}^4\text{He}$ ) as a three- (four-)nucleon resonance is ruled out by kinematic analysis. The results of a calculation, wherein the double charge exchange reaction is assumed to proceed as two sequential single charge exchange interactions, suggest that the high-energy peak is naturally explained by this double scattering mechanism. Non-static treatment of the  $\pi N$  interactions and the inclusion of nuclear binding effects appear to be important in reproducing the shape of the energy spectra at forward angles.

PACS numbers: 25.80.Ek, 25.80.Gn, 25.80.Ls, 27.10.+h

---

\*Present Address: Department of Physics, University of Colorado, Boulder, CO 80309

†Present Address: 82-1021 Kaimalu Place, Captain Cook, HI 96704

‡Present Address: School of Physics and Astronomy, Tel Aviv University, Tel Aviv 69978, Israel

§Present Address: Radiation Oncology Department, University of Michigan, Ann Arbor, MI 48109

## I. INTRODUCTION

Pion double charge exchange (DCX), a nuclear reaction in which two units of charge are exchanged between a pion and a nucleus, is an important tool with which to investigate the details of the pion-nucleus interactions as well as correlations between nucleons within the nucleus. DCX is unique among pion-nuclear scattering reactions, as it must involve at least two nucleons in order to conserve charge. Thus, the physiognomy of the DCX process revealed by the experimental cross section depends on the coordinates of two particles in the wavefunction of the nucleus. As a probe of the pion-nucleus interaction, DCX may be used to isolate contributions from different types of reaction mechanisms. Other pion-nucleus reactions appear to be dominated by single scattering mechanisms, but DCX must proceed through less simple mechanisms such as double scattering, as shown in Fig. 1(a).

An experimental investigation of DCX in  ${}^4\text{He}$  at intermediate energies (120–270 MeV) has been performed in order to study the multiple scattering mechanisms of the  $\pi$ -nucleus reaction directly. The choice of  ${}^4\text{He}$  as a nuclear target allows an investigation of DCX in an extensively studied few-body system for which microscopic treatment of the dynamics is possible in principle. At the same time, the  ${}^4\text{He}$  nucleus has a large density which may allow some effects of the nuclear medium to be investigated. The final state is also relatively simple, consisting of a pion and either four protons or four neutrons, resulting from, respectively, the reactions  ${}^4\text{He}(\pi^+, \pi^-)4p$  and  ${}^4\text{He}(\pi^-, \pi^+)4n$ .

## II. PREVIOUS EXPERIMENTAL WORK

The first investigation of DCX in  ${}^4\text{He}$  was reported by Davis *et al.*[1] in 1964. This and several subsequent measurements [2, 3, 4] of DCX cross sections in  ${}^3\text{He}$  and  ${}^4\text{He}$  were undertaken as searches for bound three- or four-neutron states using the  $(\pi^-, \pi^+)$  reaction. More broadly motivated studies of DCX in  ${}^4\text{He}$  at energies above the  $\Delta$  resonance were carried out using liquid helium bubble chambers [5, 6, 7]. In the energy range 98–156 MeV total cross section measurements were performed by Falomkin *et al.*[8, 9] using a high-pressure helium streamer chamber. Although some interesting phenomena were observed in these experiments, the limited statistics precluded quantitative conclusions. Ref. [10] contains a critical review of these and other experiments on  ${}^4\text{He}$ . Other early DCX experiments

on various nuclei which used nuclear emulsions, bubble chambers, and spark chambers as detectors are described in Refs.[11, 12].

The first modern measurement of doubly differential cross sections for inclusive DCX, using a magnetic spectrometer to detect the outgoing pions, was made at the Schweizerisches Institut für Nuklearforschung (now PSI) for the  $^{16}\text{O}(\pi^+, \pi^-)$  reaction [13]. Subsequently, the  $^4\text{He}(\pi^+, \pi^-)$  reaction was studied by Stetz *et al.*[14, 15] using the EPICS spectrometer at the Los Alamos Meson Physics Facility (LAMPF). Stetz *et al.* measured doubly differential cross sections for three incident pion energies (140, 200, and 295 MeV) at several angles in the range  $30^\circ$ – $120^\circ$ . One spectrum was a re-measurement of the spectrum reported by Kaufman *et al.*[3] at 140 MeV, and confirmed that the normalization of the older data was incorrect (too small) by a factor of 100, as had been suspected. Six additional spectra were measured with pions at the two higher incident energies, and one spectrum for the  $^4\text{He}(\pi^-, \pi^+)$  reaction was observed at 295 MeV incident energy.

Total and differential cross sections and pion momentum distributions have been measured at six energies in the 70–130 MeV range using the CHAOS detector at TRIUMF[16]. Some evidence for a  $d'$  dibaryon state of mass 2.06 GeV is claimed to be found in the energy dependence of the total DCX cross section.

An extensive study of the  $^3\text{He}(\pi^-, \pi^+)$  reaction[12] in the incident energy range 120 – 240 MeV was carried out with the same apparatus as that used in the experiment reported in this paper. The  $^3\text{He}$  data, with good statistical accuracy and complete coverage of the outgoing pion energy spectrum, revealed a double-peaked structure at forward angles [12]. This result is in striking contrast to the spectra seen in a systematic study of DCX on heavier nuclei ( $^{16}\text{O}$  to  $^{208}\text{Pb}$ ) [11], in which this structure is absent, and which roughly resemble the distribution of events in four-body phase space. A hint of this structure had been seen in the earlier  $^3\text{He}$  DCX data of Sperinde *et al.*[17], whereas it was not apparent in the  $^4\text{He}$  data of Kaufman *et al.*[3] or those of Stetz *et al.*[15].

### III. PREVIOUS THEORETICAL WORK

The first microscopic calculation of the DCX process in  $^4\text{He}$  was reported by Becker and Schmit[18], using a reaction model developed by Becker and Marić[19]. The sequential single-charge-exchange (SSCX) mechanism is calculated in a fixed-nucleon (FN) framework,

and only resonant [ $\Delta(1232)$ ] amplitudes are used to describe the  $\pi N$  interaction, with an off-shell correction factor. Total cross section predictions of this calculation are presented in Ref. [20] and they are generally too large by an order of magnitude, though the energy dependence is reminiscent of that of the data, as will be shown later. The quantitative disagreement should be expected at the very least from the use of plane waves to describe the outgoing pions, i.e., the effects of absorption and multiple scattering are not included.

Germond and Wilkin[21, 22] proposed that a major contribution to DCX might come from a pion-pion scattering mechanism, as shown in Fig. 1(b). The amplitude is calculated for a nucleon pair, drawing on the current algebra theory of Weinberg[23] for the  $\pi\pi$  interaction. The pion “cloud” between the nucleon pair is calculated with a relativistic expression derived from the pseudoscalar pion and Dirac nucleon theory described by Bjorken and Drell[24]. The relatively large total cross sections obtained fueled speculation that this mechanism was important. However, the mechanism shown in Fig. 1(c) must also be included, and it was found by Robilotta and Wilkin[25] that its amplitude cancels that of the mechanism in Fig. 1(b) to a large extent.

Jeanneret *et al.*[7] considered a model of DCX in which pion-induced pion production (PIPP) is followed by two-nucleon absorption of one of the two final pions. The calculation is a convolution of the free PIPP cross section and pion absorption cross section in deuterium ( $\pi^+d \rightarrow pp$ ), with some corrections for the available phase space. At the high energies of their experiment (1.5–2.0 GeV), the authors find general agreement of their predictions with their measured total cross sections.

The calculation of Gibbs, Gibson, Hess, and Stephenson [26] was based on the same reaction model as that of Becker and Schmit[18], but brought to bear the more sophisticated techniques pioneered by Gibbs and his co-workers [27]. It should be noted that a simpler approximation of those methods was used in the DCX calculation; specifically, the coupled scattering equations were not solved. The initial and final pion states as well as the final nucleon states were described with plane waves, although the effect of simple FSI between the spectator nucleon pair was investigated. A pion scattering amplitude from fixed nucleon positions was calculated, and then averaged by the  $^4\text{He}$  wavefunction. The final nucleon momenta were integrated over the available phase space using a Monte Carlo technique.

The total cross section predicted by this calculation is a factor of 100 smaller than that measured in the energy region 98–156 MeV by Falomkin *et al.*[8, 9]. This theoretical re-

sult is in fact consistent with the approximate agreement found with the Kaufman *et al.* measurement[3] at 140 MeV, which is now known to have been incorrectly normalized by a factor of 100. The calculation also underpredicts the  $0^\circ$  excitation function for 176 MeV pions measured by Gilly *et al.*[2] and the pion momentum spectrum measured at 485 MeV by Carayannopoulos *et al.*[5]; however, the authors [26] comment that the calculation is not expected to work well at the higher incident energies.

A series of papers containing theoretical predictions for DCX cross sections in  $^3\text{He}$  and  $^4\text{He}$  was published by Jibuti and Kezerashvili[28, 29, 30, 31, 32, 33]. Their basic approach was to expand initial and final nuclear wavefunctions in a hyperspherical basis, solving four-body equations for the  $^4\text{He}$  nucleus using various models of the  $NN$  potential. In Refs. [28, 29] these wavefunctions were used to calculate DCX cross sections in  $^4\text{He}$  using the exact same form of the double scattering operator as used by Gibbs *et al.*[26]. Surprisingly, agreement was found with both the incorrect data of Kaufman[3] and the presumably correct data of Gilly *et al.*[2]. A similar calculation for DCX in  $^3\text{He}$  was reported[30] several years later, and successfully reproduced the spectrum measured by Sperinde *et al.*[17], explaining the high energy peak evident in their data as a result of FSI. The following year Jibuti and Kezerashvili published a long report[31] describing their wavefunction formalism and calculation in some detail, drawing together their earlier work on DCX in  $^3\text{He}$  and  $^4\text{He}$ , and extending the results by including more hyperspherical basis states in their expansion of the nuclear wavefunction. In addition, the operator for the  $\pi\pi$  scattering mechanism was extracted without change from Germond and Wilkin[21] and inserted between their wavefunctions. Two predictions of DCX energy spectra – one using the  $\pi\pi$  mechanism of Germond and Wilkin and one using the SSCX mechanism of Gibbs – were compared to one of the spectra measured by Stetz *et al.*[15]. Both predictions agreed quite well with the data, and no combination of the two was discussed, in this article or in later work[32, 33].

A completely different approach to calculating inclusive reaction cross sections has been taken by several other authors[34, 35]. Cascade calculations were performed which treated the propagation of the pion through the nucleus classically, and used interaction probabilities dependent on the local nuclear density. Hufner and Thies[34] derived an approximate solution of the Boltzmann transport equation, and presented results for a number of different inclusive reactions including the total cross sections for DCX in  $^4\text{He}$ . The resonant part of the  $\pi N$  scattering amplitude was calculated non-statically, using a Fermi gas distribution to

describe the nuclear density in coordinate and momentum space. Binding effects were not included, but the resonance width was modified to account for Pauli blocking and absorption. The results of their calculation agreed qualitatively with the existing data, though they exceeded the measurement of Stetz *et al.*[14] and did not reproduce its energy dependence.

Oset and co-workers[35] have emphasized the description of the  $\Delta$ -nucleus interaction with density dependent terms calculated in nuclear matter. Their results for DCX in  $^{16}\text{O}$ ,  $^{40}\text{Ca}$ ,  $^{103}\text{Rh}$ , and  $^{208}\text{Pb}$  were compared with data in Ref. [11]. This calculation has been extended to nuclei as light as  $^6\text{Li}$ [36], although treating this system as “nuclear matter” is surely unrealistic. No calculations are available for  $^4\text{He}$ .

More recently, the Gibbs *et al.* calculation[26] was reviewed critically and modified by Rebka[37] and Kulkarni[38]. The phase space was calculated relativistically, an antisymmetrized initial wave function was used, the spin and isospin coefficients were recalculated, and the newer  $\pi$ -nucleon phase shift parametrization of Rowe, Salomon, and Landau[39] was used. This calculation yielded cross sections substantially larger than those of Ref. [26], but still failed to reproduce either the magnitude or energy dependence of the Kaufman[3] or Gilly[2] cross sections. Calculations were also performed for the doubly differential cross sections measured in the present experiment, and the results will be compared with the data in Section VII.

Kulkarni[38] also constructed a relativistic three-body model of  $\pi$ -nuclear interactions, and applied it to DCX. This calculation will be described briefly and its results compared with the present data in Section VII.

A recent paper by Alqadi and Gibbs [40] reported calculations of  $^4\text{He}(\pi^+, \pi^-)$  cross sections using two different methods: the two-nucleon sequential single charge exchange model and an intranuclear cascade code. Final state interactions were included, as well as the contribution of the pion-induced pion production process to the inclusive DCX cross sections at 240 and 270 MeV. These calculations will be discussed in Section VII.

#### IV. EXPERIMENTAL APPARATUS AND PROCEDURE

In the present experiment, the inclusive DCX processes  $^4\text{He}(\pi^+, \pi^-)$  and  $^4\text{He}(\pi^-, \pi^+)$  have been investigated by measuring doubly differential cross sections,  $d^2\sigma/d\Omega dE$ , at three to five outgoing pion laboratory angles in the range  $25^\circ$ – $130^\circ$ , for incident positive pions of

energy 120, 150, 180, 240, and 270 MeV, and for incident negative pions of energy 180 and 240 MeV. At each angle, measurements were performed for outgoing pion kinetic energies  $E$  from 10 MeV up to the kinematic limit for the reaction. Preliminary results of this experiment have been reported in Ref. [41].

The experiment was performed with incident  $\pi^\pm$  beams from the high-energy pion channel (“P<sup>3</sup>”) at LAMPF. The experimental apparatus and procedure have been discussed in detail by Wood *et al.* [11] and Yuly *et al.* [12] and will be treated only briefly here. The outgoing pions were detected using a 180° vertical bend, double focusing magnetic spectrometer, with an effective solid angle of about 16 msr and a momentum bite of about 8% (see Fig. 2). The 180° bend of the magnet provides stringent selection of the charge of the detected particle, and the short flight path (3.5 m), which was entirely in vacuum except for a 2.5 cm interruption for a mid-spectrometer wire chamber, allowed low-energy pions to reach the focal plane with minimal corrections for scattering and decay. Since no detectors are required at the entrance to the spectrometer, high luminosities could be used.

The detector system had five components: a wire chamber (WC0) placed in the mid-plane of the spectrometer, two wire chambers (WC1 and WC2) near the focal plane that were used to reconstruct trajectories, behind these, a 1.6 mm scintillator (S1), that provided an accurate time reference for the trigger as well as pulse height information useful in the identification of particles, and lastly a fluorocarbon (FC-88) Čerenkov detector that distinguished electrons from pions.

The trigger was a fourfold coincidence among the three wire chambers and the scintillator. Inclusion of the mid-spectrometer wire chamber guaranteed that a particle had passed through the spectrometer, which accomplished a crucial reduction of the trigger rate due to room background. The timing information available from this chamber was also used to distinguish pions from very slow protons.

The liquid  $^4\text{He}$  target was a cylindrical cell 25 mm in diameter and 75 mm high with a 51  $\mu\text{m}$  thick Mylar wall. It was surrounded by four layers of 0.64  $\mu\text{m}$  aluminized mylar super-insulation and, at a radius of 19 cm, a 13  $\mu\text{m}$  aluminum heat shield maintained at liquid nitrogen temperature. The insulating vacuum of the cryostat was contiguous with that of the spectrometer vacuum chamber. The top of the cell was connected to the bottom of a 30 liter reservoir, which fed liquid  $^4\text{He}$  to the target under the force of gravity.

The target cell and a CH (styrofoam) cylinder of the same dimensions were mounted



vertically on the axis of rotation of the spectrometer. An elevator mechanism could position each of the targets in the path of the beam, permitting convenient measurement of  $\pi p$  scattering, which was the reference cross section in this experiment. Background from the helium target cell walls was measured by detecting pions from the same cell after the helium had been evacuated. The measured yield from the empty cell was typically less than 10% of the yield measured when the cell contained liquid helium.

The temperature of the  $^4\text{He}$  was determined by the vapor pressure in the reservoir, which was essentially the same as the local atmospheric pressure ( $584 \pm 13$  mmHg) plus  $0.5$  lb/in<sup>2</sup> overpressure from a gas outflow meter. Interpolating from empirical measurements of liquid  $^4\text{He}$  density as a function of vapor pressure one finds a density of  $128.6 \pm 0.3$  mg/cm<sup>3</sup>. The  $^4\text{He}$  target density determination was checked in a subsequent experiment on DCX in  $^3\text{He}$  [12]. Since at temperatures below that necessary to liquify  $^3\text{He}$  (2.17K) liquid  $^4\text{He}$  becomes superfluid and no longer boils, its density is known more reliably. The density measurements reported in this paper were found to be in excellent agreement with those made subsequently with the superfluid  $^4\text{He}$  target.

Before reaching the target, the pion beam passed through an ionization chamber, which was used to determine the relative flux. Since this device was sensitive to all charged particles in the beam, it was necessary to normalize the flux measurement each time the beam transport elements were adjusted. The size (about 1.6 cm in diameter) and position of the beam spot were continuously monitored by a small multi-wire proportional chamber placed downstream of the ionization chamber and 30 cm upstream of the target. Downstream of the  $^4\text{He}$  target, the pion beam struck a 6 mm thick polyethylene ( $\text{CH}_2$ ) target. Three-element plastic scintillator telescopes were placed on each side of the  $\text{CH}_2$  target to detect pions scattered at  $90^\circ$ . These telescopes were used to monitor the position of the incident beam, as well as to provide a check on the flux determined by the ionization chamber. The response of the telescopes was sensitive essentially only to pions, since beam contaminants are very unlikely to scatter at  $90^\circ$  into the telescopes.

To measure the doubly differential cross sections the target was exposed to an incident pion beam and events were collected at given spectrometer momentum settings until statistical uncertainties of approximately 5% in the number of detected pions were achieved. Data were collected at 10 MeV intervals in outgoing pion energy. In addition to each complete set of  $^4\text{He}$  observations, a series of observations was made measuring the background from

the empty target walls. This process was repeated for each spectrometer angle and incident energy. Each time the incident energy, and hence the normalization of the beam monitors, was changed, a series of CH normalizations, that covered the same range of angles but in smaller steps, was performed.

## V. DATA ANALYSIS

The goal of this experiment was to measure a doubly differential cross section for each reaction, incident pion energy, scattering angle, and outgoing pion energy studied. The doubly differential cross section is related to observable quantities as follows:

$$\frac{d^2\sigma}{d\Omega dE} = \frac{N_{\text{det}} \epsilon_c}{N_{\text{inc}} \Delta\Omega \Delta E x \rho f_d f_l} \quad (1)$$

where  $N_{\text{det}}$  is the number of pions detected,  $N_{\text{inc}}$  is the number of pions that were incident,  $x$  is the effective thickness of the target,  $\rho$  is the density of the target,  $\Delta\Omega$  is the effective solid angular acceptance of the spectrometer,  $E$  is the outgoing pion kinetic energy and  $\Delta E$  is its range,  $\epsilon_c$  is a correction of the spectrometer acceptance due to multiple scattering and energy loss,  $f_d$  is the correction due to pion decay, and  $f_l$  is the dead-time correction.

The analysis procedure is described in detail in [10] and will only be summarized here. (See also ref[12].)

### A. Wire chamber calibration and phase space definition

Calibration constants relating time differences of signals from wire chambers to position were established by placing a collimated  $^{55}\text{Fe}$  source at precisely measured positions in front of the chambers. For each event, the position information from WC1 and WC2 was used to reconstruct the particle trajectory back to the focal plane of the spectrometer. Reconstructed trajectories were tested for conformity with the distribution in phase space of particles that could have been transmitted by the spectrometer from the target to the focal plane.

### B. Particle Identification

To calculate cross sections it was necessary to separate the pions from the other particle species that also caused triggers. Protons were generally eliminated by their large pulse

heights in the scintillator. At a spectrometer momentum setting of about 156 MeV/c, where the protons were just reaching the scintillator, however, many of the protons deposited the same amount of energy as the pions in the scintillator. At this momentum, the protons were distinguished by their longer time-of-flight between WC0 and S1.

Since pions, as well as electrons,<sup>1</sup> emit Čerenkov radiation at spectrometer settings greater than 180 MeV/c ( $T_\pi = 88$  MeV), it was not possible to use the Čerenkov detector to distinguish electrons from pions on an event-by-event basis. Instead, a statistical method was used, which is described in detail in [10] and is very similar to that described in [12].

### C. Acceptance and Dispersion

The momentum acceptance,  $\Delta p/p$ , and dispersion were determined by scanning a  $\pi^+p$  elastic scattering peak from the CH target across the spectrometer focal plane by changing the spectrometer magnetic field. The changing acceptance across the focal plane resulted in changes in the observed area of the peak. The relative acceptance as a function of focal plane position was determined by this method, and was used to correct  $N_{\text{det}}$ . The effective total momentum acceptance was determined to be about 8% by integration across the entire focal plane.

### D. Normalization

The absolute number of incident pions,  $N_{\text{inc}}$  in Eq. (1), was obtained by comparison of  $\pi p$  elastic scattering measurements from the CH target with known cross sections determined by interpolation using the energy-dependent phase shift program SCATPI [42]. In this way, the effective total solid angle,  $\Delta\Omega$ , and the effective target thickness,  $x$ , were included in this calibration. This procedure was repeated at several scattering angles for each setting of the beam transport system in order to improve the accuracy of the normalization, as well as to check for the presence of angle-dependent effects.

---

<sup>1</sup> Electrons or positrons, depending on the charge setting of the spectrometer. The word “electron” will be used generically throughout this discussion.

### E. Background Subtraction

The pions counted with the empty target were primarily those scattered from the walls of the target cell. The background was typically only about 8%, and never more than 15%, of the full-target rate, and was measured to about 30% accuracy. The measurements with the empty target were analyzed in the same manner as those with the full target, and properly normalized background data were subtracted point-by-point from the full-target data.

### F. Corrections

Corrections (see Eq. (1)) were made to account for other effects that would change the shape and magnitude of the cross section distributions. The number of pions detected was reduced by decay as they travelled from the target to the detectors. Approximately 80% of the pions survived at 200 MeV, while at 10 MeV only 30% survived. Some of the decay muons traversed the spectrometer, while others did not. In fact, it is possible for pions that would not have traversed the spectrometer to decay into muons that could. Since the detector system could not separate the muons from pions, these effects were computed by Monte Carlo methods which produced the factor  $f_d$  in Eq. (1). This procedure is described in greater detail in Ref. [11]. Muon contamination from pion decay in the spectrometer was simulated with the DECAY TURTLE [43] code. The fraction of muon contamination ranges from 1% at 10 MeV to 20% at 200 MeV outgoing pion kinetic energy. A different Monte Carlo program, MUCLOUD [10, 44], was used to simulate decays in the scattering chamber. MUCLOUD used the uncorrected cross sections in an iterative procedure to obtain the corrections, which were typically 0–30%. Energy loss and multiple scattering in the target and in WC0 changed the effective acceptance of the spectrometer; these were corrected for by the factor  $\epsilon_c$ , which was determined by simulation to be different from unity only for outgoing pion energies less than 30 MeV. The maximum value of  $\epsilon_c$  was about 1.3.

### G. Integrated cross sections

Integration of the doubly differential cross sections over outgoing pion energy yielded an angular distribution. This integration was carried out using the trapezoid rule. The cross section below the lowest measured outgoing energy of 10 MeV as found by linear

extrapolation to zero at zero outgoing pion energy. Except for several forward-angle spectra at high incident pion energy, the doubly differential cross sections were measured up to the kinematic limit for the DCX reaction, and thus the high-energy end of the integral required no extrapolation of the data. The exceptional cases were extrapolated linearly to zero cross section using the slope determined by the highest energy pair of cross section measurements. The uncertainty in each differential cross section was calculated as the sum in quadrature of the uncertainty in each trapezoid's area. The uncertainty in the extrapolation of the endpoints to zero cross section was estimated to be one-half of the contribution to the integral from the endpoint regions. In all cases these uncertainties[10] were small compared with the systematic uncertainties discussed in the next section.

The smooth angular dependence of the differential cross sections allows a simple method of integration over angle to determine a quantity which we term the “total reaction cross section.” The angular distributions between the most forward and backward angle measurements were fitted with sums of Legendre polynomials in  $x = \cos \theta_{\text{lab}}$ ; the distributions were extrapolated linearly in  $x$  from the extreme angle measurements to  $0^\circ$  and  $180^\circ$ , using the derivative of the Legendre polynomial sum at the extremes to define the slopes. The uncertainty in the total reaction cross section was determined by fitting the Legendre polynomials to the angular distribution plus and minus the uncertainty at each angle. This uncertainty and that in the extrapolation [10] were less than or comparable to the systematic uncertainties discussed in the next section.

## H. Systematic uncertainties

There are systematic uncertainties of three types: those that depend on the energy of observation, the angle of observation, and the overall normalization. The uncertainty that depends on the energy of observation includes contributions from the electron-pion separation procedure, which were between 2% and 5%, together with contributions from estimates of the corrections for energy loss and multiple scattering in the target and in the mid-spectrometer wire chamber, and for effects of pion decay and muon contamination, which contributed an additional 5%. The uncertainty in the correction for energy loss and multiple scattering was estimated to be equal to one-half of the correction applied. The uncertainty in the corrections for pion decay and muon contamination was estimated to be one-half of

the difference between the correction derived from the simulation described earlier, and that given by accounting only for the loss of pions by decay within the spectrometer.

An angle-dependent uncertainty (see Table I) arises from possible misalignment between the axis of the target and that of the spectrometer, which will produce changes in both the thickness of the liquid  $^4\text{He}$  seen by the beam and in the effective acceptance of the spectrometer. These uncertainties were estimated together by comparison between the observed angular variation of the differential cross section for  $\pi p$  scattering and that predicted from interpolation of the known cross sections.

Normalization uncertainties are of two kinds; those that are due to slowly varying changes in the response of the ionization chamber used to monitor the incident beam flux and the density of the  $^4\text{He}$  target, and those that involve the determination of the absolute scale of the measured cross sections by normalization to  $\pi p$  scattering. Variation in the ionization chamber response, due to changes in ambient temperature and pressure, was monitored by comparison with the primary proton beam monitor and a downstream scattering monitor [10]. Since these variations were observed to occur on roughly the same time scale as did changes of spectrometer angle, they have been included with the angle-dependent uncertainty.

The uncertainty in the overall scale of the cross section contains contributions from uncertainties in the densities of the  $^4\text{He}$  and CH targets and in the assumed  $\pi p$  scattering cross section. The uncertainties in the densities were determined [10] to be 0.7% and 0.6% for the  $^4\text{He}$  and CH targets, respectively. An additional overall uncertainty of 2% is assumed to account for the accuracy of the phase shift prediction of the free  $\pi p$  cross section[42]. Combining these uncertainties with the uncertainty in the determination of each particle's position in the spectrometer focal plane (1%) and in the determination of the spectrometer acceptance function (1%), yields an overall uncertainty of 2.4%, independent of incident beam energy and angle. (The uncertainties due to the determination of electronics deadtime, spectrometer dispersion, and wire chamber efficiency were insignificant compared to those listed above.) This uncertainty has been combined in quadrature with the angle-dependent uncertainties in Table I to yield the final result in the last column for each incident beam.

## VI. RESULTS

### A. Doubly Differential Cross Sections

The doubly differential cross sections measured for the  ${}^4\text{He}(\pi^+, \pi^-)$  reaction at incident energies 120, 150, 180, 240, and 270 MeV are presented as pion energy spectra in Figs. 3–7, respectively. The doubly differential cross sections measured for the  ${}^4\text{He}(\pi^-, \pi^+)$  reaction at incident energies of 180 and 240 MeV are displayed in Figs. 8 and 9. The bars on the plotted points indicate the statistical uncertainty plus the systematic uncertainty in the pion-electron separation procedure and the corrections for pion decay, energy loss in the target cell, and multiple scattering in the inter-dipole wire chamber.

#### 1. Contribution from Pion-Induced Pion Production

The detection of a pion with charge opposite to that of the incident beam is not a unique signature of DCX at incident energies above about 170 MeV, the threshold for the pion-induced pion production (PIPP) reactions  ${}^4\text{He}(\pi^+, \pi^+\pi^-)pppn$  and  ${}^4\text{He}(\pi^-, \pi^-\pi^+)pnenn$ . The magnitude and kinematic range of the contribution of PIPP is severely limited by the phase space available to this reaction, however, and a significant effect is only possible at incident energies well above 200 MeV.

To indicate the effect that this contribution might have on the shape of the DCX energy spectra, Figs. 6 and 7 illustrate the position of the upper limit of outgoing pion energy from PIPP as well as the shape of the available phase space for the reaction  $\pi^+ + {}^4\text{He} \rightarrow {}^3\text{He} + \pi^+ + \pi^- + p$ , for the spectra measured at incident energy 240 and 270 MeV. The phase space predictions, whose normalization will be discussed later, are only presented as a guide. (The shapes of the energy spectra from PIPP in deuterium[45] were found to be very similar to phase space, but the measurement of Grion *et al.*[46] of PIPP in  ${}^{16}\text{O}$  found significant deviation from such predictions.)

#### 2. Comparison with Phase Space Predictions

In earlier measurements, Wood *et al.*[11] found that a general feature of the doubly differential cross sections for inclusive DCX in  ${}^{16}\text{O}$  and  ${}^{40}\text{Ca}$  was the similarity of the shapes

of the energy spectra to simple predictions based on the available phase space in a DCX reaction leading to four bodies: a pion, two knocked-out nucleons, and residual nucleus. Figure 10 compares the inclusive spectra from the  $^4\text{He}$  and  $^{16}\text{O}$  DCX reactions, measured at  $25^\circ$  and incident energy 240 MeV; the different curves represent phase space energy distributions based on different numbers of particles in the final state. The phase space prediction for the  $^{16}\text{O}$  data assumes four bodies in the final state, as mentioned above; this curve has been normalized so that the phase space prediction integrated over the solid angle and energy of the outgoing pion yields the measured total DCX reaction cross section. The three predictions compared with the  $^4\text{He}$  spectrum are similarly normalized to the total cross section predicted by a simple scaling law[47]. The dashed curve is the result for a 5-body final state for the DCX reaction  $\pi^+ + ^4\text{He} \rightarrow \pi^- + p + p + p + p$ , which is in fact the ultimate final state. The solid and dot-dashed curves correspond to 4- and 3-body final states which might result if two or three of the nucleons in the final state recoil as a “cluster” with no internal motion, i.e.,  $\pi^+ + ^4\text{He} \rightarrow \pi^- + p + p + (2p)$  or  $\pi^+ + ^4\text{He} \rightarrow \pi^- + p + (3p)$ . It is clear that, unlike the case of  $^{16}\text{O}$ , none of the distributions even approximately represents the data, nor provides any insight into the most striking feature of the doubly differential cross sections for DCX in  $^4\text{He}$ , the large peak-like structure at high outgoing pion energy.

### 3. *Kinematic Analysis of the Energy Spectra*

In order to gain more quantitative information about the shape of the energy spectra, especially the centroid energy and width of the high energy peak, a line shape constructed from a Gaussian curve and a five-body phase space distribution was fitted to those spectra in which a peak was apparent. The centroid, width, and area of the Gaussian were all allowed to vary in the fitting procedure, but only the magnitude of the phase space distribution was variable. The missing mass and four-nucleon excitation energy (defined as the missing mass less the mass of the four free nucleons in the final state) was extracted from this analysis. Examination of the results (see Ref.[10]) clearly indicates that the peak does not correspond to a resonance in the four-nucleon system. There exists a systematic variation in the missing mass with scattering angle and incident energy which is well outside the uncertainty in its



determination.<sup>2</sup> The width of the peak varies less dramatically, but nonetheless sufficiently to contradict the four-nucleon resonance hypothesis.

Another hypothesis is that the peak results from quasi-free scattering of the pion with some sort of “cluster” within the nucleus. If the mass of the cluster remains unchanged by the scattering, there is no choice of mass which can describe the magnitude and angular variation of the peak energy, even at a single incident energy. If one allows the mass of the cluster to change, corresponding for example to the excitation of the cluster into a resonant state, it is possible to find a combination of initial mass and excitation energy which approximately describes the data at a given incident energy. It should be emphasized that a similar variation results if the scattering predominantly occurs on a certain number of nucleons, and energy is lost to each nucleon individually. The quasi-free kinematic analysis presented here is similar in this sense to earlier rapidity analyses of inclusive energy spectra[11, 48, 49]. Ref. [10] presents the results of fitting the kinematic variation with two-body scattering formulae, assuming an initial cluster “mass” and a final “mass” found by adding an excitation energy to the initial mass. The initial masses are poorly constrained, but nevertheless show a large variation with incident energy, as do the excitation energies which are more accurately determined. An explanation of the high outgoing energy peak in terms of quasi-free scattering and excitation therefore seems unlikely.

In Section VII.B a simple double scattering reaction model is considered; the results suggest that this peak has a natural explanation in the dynamics of two forward angle  $\pi - N$  reactions.

#### 4. Comparison of ${}^4\text{He}(\pi^+, \pi^-)4p$ and ${}^4\text{He}(\pi^-, \pi^+)4n$ Reactions

To the extent that Coulomb effects may be neglected,  $(\pi^+, \pi^-)$  and  $(\pi^-, \pi^+)$  are identical reactions in nuclei with equal numbers of protons and neutrons, assuming the invariance of the strong interaction with respect to rotations in isospin space. Figures 11 and 12 compare a sample of the energy spectra for the two reactions. The error bars indicated in the figure do not include the uncertainty in the normalizations which are 6% and 7% for the 180 and

---

<sup>2</sup> For example, the excitation energy at  $25^\circ$  varies from  $38.1 \pm 0.6$  MeV at incident energy 150 MeV to  $86.1 \pm 0.9$  MeV at 270 MeV; and at incident energy 240 MeV from  $74.4 \pm 0.7$  MeV at  $25^\circ$  to  $93.8 \pm 2.5$  MeV at  $130^\circ$ .

240 MeV spectra, respectively. As can be seen, the shapes and magnitudes of the spectra are quite similar.

This near equality of the cross sections for these mirror processes can be understood by estimating the sizes of effects caused by the Coulomb force[10]. It is found that the distortion of the pion wave causes a shift of at most 6 MeV in the  $\pi$ -nucleus interaction between the two reactions. The effect of the Coulomb energy on the distribution of the nucleons in the  ${}^4\text{He}$  ground state is estimated to produce a difference of about 1 MeV between the neutron and proton distributions.

The energy of the four-nucleon final state is affected more strongly by the Coulomb potential; the potential energy difference between four protons and four neutrons is approximately 12 MeV. Thus, reactions leading to states of four protons with minimum internal motion could be suppressed or their energy shifted relative to four-neutron states, because of the Coulomb energy barrier. On the other hand, the energy of the first excited state of  ${}^4\text{He}$  indicates the effective “strength” of the Pauli principle to be about 20 MeV. Two nucleons must be excited out of initial  $l = 0$  eigenstates in  ${}^4\text{He}$  by the DCX reaction, giving a total energy barrier of approximately 40 MeV for a four-like-nucleon “ground state.” Since the Pauli principle applies to both four-proton and four-neutron final states, the Coulomb potential energy difference therefore appears to be less significant, though not negligible, in comparison with the effect of the Pauli principle. It should be noted that Coulomb effects are expected to be sizable only at the highest outgoing pion energies, which correspond to little energy left in the residual system of four nucleons.

### 5. Comparison with DCX in ${}^3\text{He}$

Figure 13 compares the doubly differential cross sections for the reactions  ${}^3\text{He}(\pi^-, \pi^+)$  and  ${}^4\text{He}(\pi^-, \pi^+)$  measured at  $50^\circ$  and 240 MeV incident energy. The shapes of the energy spectra are strikingly similar. The magnitude of the DCX cross sections in  ${}^3\text{He}$  is slightly larger than in  ${}^4\text{He}$ , and the peak is at a somewhat higher outgoing pion energy. The latter difference between the two spectra may arise simply from the difference in binding energies of the nuclei, since the DCX reaction leads to complete disintegration of the nucleus in both cases.

The difference in the magnitude of the differential cross sections may result from the

different strengths of the competing reactions of quasi-free scattering and pion absorption. Recalling that negative pions interact more strongly with neutrons (in the  $\Delta$  resonance region), the competition from quasi-free scattering in  $^4\text{He}$  should be twice as large as in  $^3\text{He}$ . Likewise, if one considers pion absorption to proceed through a “quasi-deuteron” mechanism, twice as many  $np$  pairs are found in  $^4\text{He}$  as in  $^3\text{He}$ . Indeed, recent measurements of pion absorption cross sections in  $^3\text{He}$  and  $^4\text{He}$  [50] show the latter cross section to be approximately twice the former, in the  $\Delta$  resonance region. Thus, the absorption process is expected to compete more strongly with DCX in  $^4\text{He}$ . However, the DCX reactions should also be sensitive to the density of the nucleus. One expects double scattering to be enhanced if the average internucleon distance is smaller in one case compared to another, suggesting a larger DCX reaction cross section in  $^4\text{He}$  than in  $^3\text{He}$ . Thus, it is not obvious how large a difference, if any, should be expected between the magnitudes of the DCX cross sections, without a more quantitative investigation of the problem.

#### 6. Comparison with Previous Measurements

Of the previous experiments[2, 4, 8, 9, 14, 15] which have investigated the DCX reaction in  $^4\text{He}$  in the energy region of the present experiment, only one[14, 15] affords the possibility of comparison with the present results for the doubly differential cross sections. Two experiments[2, 4] were searches for tetra-neutron bound states, performed for a limited range of incident and outgoing pion energies at a scattering angle of  $0^\circ$ . We note, however, that the magnitudes of the cross sections measured in both of the search experiments are consistent with the magnitude of the doubly differential cross section presented here.

Comparison of the present data with those of Stetz *et al.*[15] is problematical, since no spectra were measured at a common incident energy and scattering angle. In Ref. [10] the Stetz *et al.* data are compared with results of the present experiment at nearly the same scattering angle but for incident energies above and below, thus “bracketing” the earlier data. The comparison of the Stetz data at 140 MeV with the present data at 120 and 150 MeV (Figs. 3 and 4) shows reasonable consistency in the upper region of the pion energy spectrum, but the Stetz spectrum has a very different shape at lower pion energies. The comparison of the Stetz data at 200 MeV with the present data at 180 and 240 MeV (Figs. 5 and 6) reveals a disagreement in both magnitude and shape. The reason for this discrepancy

is not known, although some possible causes are suggested in Ref. [10].

In the present experiment neither the uncertainty arising from the normalization of the data to elastic  $\pi p$  scattering nor that arising from the corrections that depend upon outgoing pion energy is sufficient to explain the discrepancies.

### B. Differential Cross Sections

The singly differential cross sections (angular distributions) resulting from integration of the pion energy spectra as described in Sect. V.G are displayed in Fig. 14. The angular distributions for the  $(\pi^+, \pi^-)$  and  $(\pi^-, \pi^+)$  reactions are seen to be essentially identical in shape and magnitude at 240 MeV. At 180 MeV the differential cross section for  $(\pi^+, \pi^-)$  is slightly larger and more forward-peaked than that for  $(\pi^-, \pi^+)$ .

### C. Total Reaction Cross Sections

The total reaction cross sections obtained as described in Sect. V.G are given in the second column of Table II and are displayed in Fig. 15. The cross sections for the  $(\pi^+, \pi^-)$  and  $(\pi^-, \pi^+)$  reactions are seen to be essentially identical at 240 MeV, whereas the former slightly exceeds the latter at 180 MeV.

The DCX cross section does not exhibit a resonance shape near the energy of the  $\Delta$  resonance, in contrast to other pion-nucleus reactions. This can be understood as a simple consequence of double scattering, if on average the pion loses substantial energy in its first interaction. As the incident pion energy moves through the  $\Delta$  resonance, the energy of the second collision is still below resonance, whereas at incident energies 10–100 MeV higher than the  $\Delta$  resonance, the energy of the second collision is just passing through the  $\Delta$  region. The effect is to broaden the resonance and shift its maximum to higher energy. The total DCX cross section presumably falls at higher energy, as both collisions occur at energies above that of the  $\Delta$  resonance. Previous measurements at higher energies[5, 7] do indeed support this hypothesis.

### 1. Contribution of pion-induced pion production

PIPP is commonly expected to occur on a single nucleon in a quasi-free manner; the measurements in deuterium performed by Piasetzky *et al.*[45] support this hypothesis. In heavier nuclei, the effect of absorption and other competing  $\pi$ -nucleus reactions and of the nuclear medium should be taken into account. The procedure often followed to estimate the nuclear PIPP cross section is to multiply the free PIPP cross section by an “effective” number of protons or neutrons, which can be derived from analysis of the angular distribution of inclusive quasi-free pion scattering[10]. Precise data on the  $\pi^-p \rightarrow \pi^-\pi^+n$  cross section have been reported by Bjork *et al.*[51] in the incident energy range 203 – 357 MeV. The observed[45] equality of the  $\pi^+d \rightarrow \pi^+\pi^-pp$  and  $\pi^-d \rightarrow \pi^-\pi^+nn$  cross sections, and of the  $\pi^-d \rightarrow \pi^-\pi^+nn$  and  $\pi^-p \rightarrow \pi^-\pi^+n$  cross sections, justifies using the results of Bjork *et al.*[51] for both positive and negative incident pions. The PIPP cross section at 180 MeV was estimated from an extrapolation of the data of Kernel *et al.*[52], which is consistent with the model-independent fit, using four isospin amplitudes, of Burkhardt and Lowe[53]. Taking the effective numbers of nucleons for  ${}^4\text{He}$  from Ref.[10], one obtains the PIPP cross sections given in the third column of Table II. An alternative estimate of PIPP in  ${}^4\text{He}$  may be obtained from data on the  ${}^3\text{He}(\pi^+, \pi^-)$  process, which cannot proceed via double charge exchange. This cross section was measured at 240 MeV incident energy at two angles ( $25^\circ$  and  $130^\circ$ ) by Yuly *et al.*[12]. If one assumes that the angular distribution of PIPP in  ${}^3\text{He}$  is similar to that in  ${}^2\text{H}$ , one can use the results in Ref.[45] to estimate a total cross section for the former process. Multiplying this result by two<sup>3</sup> to account for the extra neutron in  ${}^4\text{He}$  gives the result shown in the fourth column of Table II, which is roughly consistent with the corresponding result in the third column. Subtracting the cross sections given in the third column from the measured  ${}^4\text{He}$  inclusive cross sections yields the “corrected” DCX cross sections given in the fifth column.

The phase space distributions in Figs. 6 and 7 are normalized so as to yield the total PIPP cross sections in the third column of Table II.

---

<sup>3</sup> Use of this factor implicitly assumes that absorption, final-state interactions, and Pauli blocking effects are the same for  ${}^3\text{He}$  and  ${}^4\text{He}$ .

## 2. Comparison with other measurements

Falomkin *et al.*[8, 9] have reported total reaction cross sections in the energy region between 98 and 156 MeV. However, these measurements are statistically inaccurate, and may also suffer from an unknown systematic error (see Ref.[10]). However, within their limited accuracy, the magnitudes of these total cross sections are in overall agreement with those derived from the present data. The more accurate total cross sections reported by Stetz *et al.*[14] appear to be systematically lower than the present results by approximately 30-50%. This difference is greater than the uncertainties arising from normalization and integration in both experiments (see Ref. [10]).

The total cross section resulting from the more recent measurement of Gräter *et al.*[16] is in good agreement with the present results where the two data sets overlap at 120 MeV.

## 3. Comparison with theoretical calculations

Several theoretical predictions for the total cross section have been reported. The prediction of the sequential single charge exchange calculation of Becker and Schmit[18] (the region between the two curves labeled B-S in Fig. 15) is clearly of the wrong magnitude, and rises more rapidly with incident energy than does the measured total cross section. This is presumably because of the lack of any treatment of the effect of pion absorption, through distorted waves for example, as well as the neglect of binding effects and the use of the fixed nucleon approximation. The prediction of Germond and Wilkin[21] (curve labeled G-W in the figure), based on pion scattering from virtual pions exchanged by the nucleons (see Fig. 1(b)), has an energy dependence more similar to that of the data, but is low by a factor of approximately three. Recalling that this calculation does not include the effects of important cancelling terms in the reaction amplitude, the real contribution from such meson exchange mechanisms for DCX is expected to be even smaller. The prediction of Hüfner and Thies[34](curve labeled H-T in Fig. 15) also assumed a multiple scattering type of DCX reaction mechanism. The cross sections are calculated with a cascade approach to pion-nucleus scattering wherein the pion propagates classically between collisions. The effects of the competition of the DCX reaction with pion absorption and inelastic scattering are included in the calculation, and these effects are expected to be critical to obtaining quanti-

tative understanding. Indeed, the results of the calculation are in relatively good agreement with both the magnitude and the energy dependence of the cross sections presented here. Below 200 MeV incident pion energy, the calculation lies 10–30% higher than the measured cross sections, whereas it begins to fall below them at higher incident energies. Some of this discrepancy at higher energy may be the result of the contributions to the measured cross section from pion-induced pion production, as suggested in the figure, but the theoretical prediction appears nonetheless to be low.

## VII. COMPARISON OF DOUBLY DIFFERENTIAL CROSS SECTIONS FOR DCX WITH THEORETICAL MODELS

### A. Fixed-Nucleon Sequential Single Charge Exchange Model

With the aim of calculating doubly differential cross sections with which the present data could be compared, Rebka and Kulkarni[37, 38] reviewed and modified the fixed-nucleon SSCX calculation of Gibbs *et al.*[26], as described in Section III. The results for  ${}^4\text{He}(\pi^+, \pi^-)$  at incident energy 240 MeV and outgoing pion angles  $25^\circ$  and  $50^\circ$  are shown in comparison with the data in Fig. 16. More recently, Alqadi and Gibbs[40] have performed a fixed-nucleon calculation and investigated the effect of inclusion of final state interactions (FSI). Although differing somewhat in magnitude, the two calculations[38, 40] without FSI yield qualitatively similar results (compare Fig. 16 with Fig. 1 in Ref.[40]). The effects of FSI are seen [40] to be largest for high pion energies. This is expected, as pointed out by Alqadi and Gibbs, since in this region the relative momentum of the two final state nucleons is smallest. None of these calculations reproduce the magnitude or the shape of the doubly differential cross section. The discrepancies between the data and the modified Gibbs calculation are found to persist at other angles and incident energies [38].

### B. Non-Static Sequential Single Charge Exchange Model

At the time of the completion of the present experiment, there were no published theoretical doubly differential cross sections or angular distributions for DCX in  ${}^4\text{He}$  with which the data could be compared. However, several authors had performed simple calculations in

order to gain some understanding of the general features of the data. Wood[44] developed a simple cascade model to describe DCX in  $^{16}\text{O}$ . The scattering probabilities per unit volume were derived by averaging the free  $\pi N$  cross sections over a Fermi gas nuclear momentum distribution. While the doubly differential cross sections were similar in shape and magnitude to the data, the angular distribution and the energy dependence of the total cross section were not well described[11]. A simpler calculation, also described in Ref. [44], consisted of a folding of two free SCX cross sections, assuming a Fermi gas model of the nucleus. Pauli blocking and Fermi motion effects were investigated and found to be important. A similar folding calculation by Thies[54], using Gaussian wavefunctions to describe  $^4\text{He}$ , found very similar results. Van Loon[55] attempted to include the medium effects by parameterizing the energy spectra from inclusive quasi-free scattering and using the results in a folding calculation to obtain DCX spectra; the inclusive scattering was corrected by the ratio of the free  $\pi N$  cross sections to obtain the effective inclusive SCX spectrum, since no inclusive SCX data were available for  $^4\text{He}$ .

The major finding of Wood, Thies, and van Loon was that a high energy peak and a low energy peak in the forward angle DCX energy spectrum result from the  $(1 + 3 \cos^2 \theta)$  angular dependence of the  $\pi N$  cross section near the  $\Delta$  resonance. This shape leads to enhanced forward and backward scattering. Two forward scatterings yield a forward-going pion of high energy, and two backward scatterings also yield a forward-going pion, with much lower energy. At larger angles, the favored combinations of individual forward and backward scatterings are not as clearly separated kinematically, hence the double-peaking feature is not as clear. The cascade calculation of Wood suggests that absorption and higher-order multiple scattering obscure these features in  $^{16}\text{O}$ ; the comparison of the simpler folding models with the  $^{3,4}\text{He}$  data is however more favorable, and suggests that development of the folding calculations would be worthwhile. With this in mind, and also in the belief that proper treatment of the Fermi motion and binding effects would be important, we undertook a calculation based on the SSCX mechanism.

This treatment is an extension of some of the work of van Loon[55] and relies on the formalism developed by Thies[56] to describe inelastic, multistep reactions with quantum-mechanical transport theory. A number of approximations and assumptions are made, some of which are known to be quantitatively inaccurate in the precise description of pion-nucleus scattering, especially in the energy region of the  $\Delta$  resonance; this calculation in no way



aspires to be an exact description of pion double scattering, but its qualitative features may elucidate the important physics of the reaction.

A brief summary of the essential features of the calculation is given in Ref. [12]; an extended description is contained in Ref. [10]. The technical details will be published elsewhere[57].

In this model the incident pion interacts sequentially with two like-charge nucleons only, and thus only the leading, or “double scattering”, term in the transition matrix is used, *i.e.*,

$$T = \sum_{i=1}^A \sum_{j \neq i}^A t_i G_0 t_j, \quad (2)$$

where the  $t_i$  are the in-medium transition operators ( $t$ -matrices) for scattering from the  $i$ th nucleon, and  $G_0$  is the in-medium pion propagator. What distinguishes this calculation from simpler folding models is the non-static treatment of the  $\pi N$  interaction and the inclusion (albeit approximate) of the binding of the nucleons.

In the energy region of the  $\Delta$  resonance, the interaction between the pion and the nucleon varies strongly with pion-nucleon relative energy. Because of the the Fermi motion of the bound nucleon, the treatment of the interaction within the nuclear medium is a critical part of any calculation of pion-nucleon scattering. In particular, one wishes to account for the variation in interaction energy due to simple kinematics and the mean nuclear potential, both of which are well known. Following the treatment by Lenz[58], we replace the in-medium  $t$ -matrix by the free  $\pi N$   $t$ -matrix evaluated at an effective relative energy:

$$t_i(E) = t_{\text{free}}(E - T_{\text{c.m.}} - U(\mathbf{r}_i) - H_{A-1}), \quad (3)$$

where  $H_{A-1}$  is the nuclear Hamiltonian with the dependence on the  $i$ th nucleon separated out,  $T_{\text{c.m.}}$  is the center-of-mass kinetic energy of the system formed by the  $i$ th nucleon and the incident pion, and  $U(\mathbf{r}_i)$  is the mean nuclear (shell-model) potential felt by the  $i$ th nucleon. As discussed in Ref. [10], the dependence of the shell-model potential on  $\mathbf{r}_i$  makes a general solution intractable; here the shell model potential will be replaced with a constant,  $U_i$ . Three choices of  $U_i$  were investigated, -55 MeV, 0 MeV, and -37 MeV, corresponding to values of  $U(r_i)$  in the nuclear interior, the surface, and the wavefunction-averaged value ( $\langle {}^4\text{He} | U(\mathbf{r}_i) | {}^4\text{He} \rangle$ ), in which harmonic oscillator functions fitted to the elastic charge form factor were used. To avoid this approximation, a full  $\Delta$ -hole calculation [59, 60] would be necessary, which is beyond the scope of the present work.

Proper treatment of the off-shell momentum dependence requires a model of the  $\pi N$  interaction; typically, the off-shell effects are described with form factors which are functions of the relative momentum, and the individual  $\pi N$  partial waves are treated separately[58, 60]. In this work, these off-shell form factors are not included; the free  $t$ -matrix is calculated given the effective relative energy and the scattering angle in the center-of-mass system.

This modified free  $t$ -matrix is inserted into Eq. (2) in order to calculate the exclusive DCX amplitude. The undetected nucleon momenta are then integrated over to obtain the inclusive cross section. To simplify the computation, however, the intermediate pion is constrained to propagate classically through the nucleus. The expression for this propagator is found using a Wigner transformation [10, 56, 57] and taking the classical limit  $\hbar \rightarrow 0$ . Selecting the specific amplitude for scattering from nucleon 1 to nucleon 2, as is shown in Fig. 17, we may write

$$A_{f0}(\vec{k}', \vec{p}'_1, \vec{p}'_2, \vec{k}) = \int d^3q \int d^3p_2 \langle \vec{k}', \vec{p}'_2 | t_2 | \vec{q}, \vec{p}_2 \rangle \langle \vec{p}_2 | \phi_{1s} \rangle \quad (4)$$

$$\times \frac{1}{E - q^2/2m_\pi - (p'_1)^2/2M_N - E_1} \int d^3p_1 \langle \vec{q}, \vec{p}'_1 | t_1 | \vec{k}, \vec{p}_1 \rangle \langle \vec{p}_1 | \phi_{1s} \rangle,$$

where  $E_1$  is the energy of nucleon 1. This amplitude is calculated numerically.

Several further simplifications have been made. Within a distorted wave impulse approximation (DWIA) approach, Thies[61, 62] has shown that the inclusive quasi-free ( $\pi, \pi'$ ) reaction may be largely explained with a one-nucleon knockout mechanism, where the residual nucleus is described by the appropriate hole state. Making the same assumption here, the sum over intermediate nuclear states is restricted to a single state. The further approximation is made of describing the initial state nucleus with the shell model; since the final state of  $^4\text{He}$  after DCX is four free nucleons, the shell model may not be an apt description. However, to do better one would need to solve the four-body nuclear Hamiltonian exactly. Finally, an enormous calculational simplification is gained by replacing all of the distorted wave continuum states (nucleon and pion) with plane waves.

The general result can be further simplified by considering its application to the specific case of  $^4\text{He}$ . Since the final nuclear states will involve large excitation energies, the effect of the overall antisymmetrization of the four-nucleon states is presumed small, except for the lowest nucleon energies. By requiring that the momentum of the struck nucleon lie outside the Fermi surface of the ground state, one effectively includes Pauli blocking of the low energy nucleons, which is the major effect of the antisymmetrization. The ground state

of  ${}^4\text{He}$  is assumed then to be described by the product of four ( $1s$ ) harmonic oscillator wavefunctions.

In the calculation of the inclusive cross section, corrections have been included for the effects of nuclear recoil and center-of-mass motion. Applying the latter correction to the harmonic oscillator wavefunctions for  ${}^4\text{He}$ , it is found[10] that the size parameter  $1/b^2$  must be replaced by  $4/(3b^2)$ . The value  $b = 1.36$  fm was determined from low momentum transfer electron scattering data [63]. The free transition matrix element used in the present calculation was derived from the free  $\pi N$  cross section predicted by Arndt [64], which is an empirical energy-dependent phase-shift representation of the cross sections.

Figure 18 compares the results of the calculation with the DCX energy spectrum measured at  $25^\circ$  for 240 MeV positive pions. The solid curve corresponds to an average nuclear potential equal to  $-55$  MeV for both scatterings, i.e.  $U_1 = U_2 = -55$  MeV. The dot-dashed curve corresponds to scattering with zero potential,  $U_1 = U_2 = 0$ , and the long dashed curve corresponds to  $U_1 = U_2 = -37$  MeV, the expectation value of the potential. All three of these curves resemble the shape of the energy spectrum, while the reproduction of the position of the high energy peak possibly favors the full potential of  $-55$  MeV. As a further investigation of the effect of the different potentials, the dotted curve corresponds to  $U_1 = -55$  MeV,  $U_2 = 0$ , and the short-dashed curve corresponds to  $U_1 = 0$ ,  $U_2 = -55$  MeV. The shape and magnitude of the prediction are evidently sensitive to the choice of potential for each scattering; the critical nature of the  $\pi N$   $t$ -matrix energy prescription is therefore underscored. This sensitivity is further illustrated by the double-dot-dashed curve, which assumes the nucleons to be at rest when calculating the interaction energy (static prescription), and  $U_1 = U_2 = 0$ . The static prescription fails to reproduce the low-energy shape of the spectrum, but the position of the high-energy peak agrees relatively well with the data.

One can understand the difference between the static and non-static calculations by considering the difference between the shape of the free  $\pi N$  angular distribution in the laboratory and center-of-mass (c.m.) frames. The symmetric  $(1 + 3\cos^2\theta)$  c.m. angular distribution at  $\Delta$  resonance energies becomes forward-peaked in the laboratory. The cross section at forward laboratory angles resulting from the static prescription “uses” the laboratory angular distribution in every collision, and thus only two forward scatterings are preferred and only the high energy peak results.

The non-static prescription includes the effect of the Fermi motion of the nucleons, and also, as mentioned previously and discussed more fully by Thies[61, 65], the strong energy dependence of the  $\pi N$  interaction. This strong energy dependence leads to a preference for the  $\pi N$  interaction to occur with nucleons such that the relative energy is near the energy of the  $\Delta$  resonance. In double scattering, the enhancement of one frame over another will affect the relative size of the low and high energy parts of the DCX spectra at forward angles.

Figure 19 shows a comparison of the calculation with the data for 240 MeV incident energy at scattering angles  $25^\circ$ ,  $50^\circ$ ,  $80^\circ$ ,  $105^\circ$ , and  $130^\circ$ , for the three values of  $U_1 = U_2$ . It is seen that, as the scattering angle increases, the shape as well as the magnitude of the predictions becomes less similar to the measured cross sections. The chief defect in the shape appears to be that the calculated spectra are concentrated in too narrow a range of outgoing pion energy. The choice of the value of the potential does move the predictions over the broader range of the data, but there appears to be no one choice, even allowing  $U_1 \neq U_2$  (see Ref. [10]) that produces agreement.

The variation in the shape of the outgoing pion energy spectrum with incident pion energy is fairly well reproduced by the calculation, as illustrated in Fig. 20, which shows the  $25^\circ$  doubly differential cross section at 120, 150, 180, 240, and 270 MeV. Calculated cross sections are shown for three choices of the potentials  $U_1 = U_2$ . In each case the theoretical predictions has been renormalized to yield the same integrated area as that of the measured energy spectra. The inclusion of a non-zero potential appears to be important to determining the correct shape in most of the spectra. The comparisons shown in Fig. 20 disguise the fact that the calculation is not able to reproduce the incident energy dependence of the magnitude of the cross section – see Fig. 21. Only the prediction with  $U_1 = U_2 = 0$  has an energy dependence at all similar to that of the data. The inclusion of distortion of the pion waves is expected to cause a large reduction in the cross section, especially below the energy of the  $\Delta$  resonance where pion absorption is an important channel, along with quasi-free scattering.

### C. DCX Cross Section using Relativistic Three-Body Model

The qualitative and semi-quantitative success of the calculation described above in reproducing the data indicates that nucleon motion and nuclear binding effects are important,

although these effects were included in a somewhat *ad hoc* fashion. Ideally, the calculation should include a proper treatment of the initial nucleon motion and nucleon recoil, along with use of relativistic pion and nucleon kinematics, a full integration over the intermediate pion momentum, and incorporation of nuclear binding by means of a model which would also fix the energy arguments of the  $\pi N$   $t$ -matrix elements. Progress toward these goals was made by Kulkarni[38], who developed a relativistic three-body model of pion-nuclear interactions – the three bodies being the pion, the  $i^{\text{th}}$  nucleon, and the residual nucleus or “core” – in order to take account of medium modifications of  $\pi N$  interactions. He has calculated doubly differential cross sections for DCX based on the SSCX mechanism, with the  $\tau$ -matrix elements for the first scattering obtained from the three-body model. An attractive square well potential is used to model the interaction between the  $\pi N$  composite and the core. The energy arguments of the  $t$ -matrix elements entering the approximate expression for the  $\tau$ -matrix elements are fixed by means of this prescription, which reduces to the prescription of Garcilazo and Gibbs[66] in the non-relativistic limit.

Various investigations were performed[38]: cross sections were calculated with and without the medium-dependent terms, with different widths of the the initial gaussian nuclear wave function, and with only  $s$ -waves and only  $p$ -waves in the  $\pi N$  interaction. The relative contributions of non-spin flip, single- and double-spin-flip processes to the cross section were calculated. Somewhat surprisingly, the inclusion of medium-dependent terms was seen to have only a small effect on the cross section. The double-peaking in the forward-angle cross sections was confirmed to arise from the  $p$ -wave component of the  $\pi N$  interaction, as expected from previous work[44].

Reference[38] contains comparisons of the relativistic three-body model calculation with a large number of the cross sections measured in the present experiment. In general, the agreement is poor, with the exception of the case at 120 MeV, where the theory reproduces both the shape and magnitude of the measurements. A typical result of this calculation is shown in Fig. 22, which can be compared with Fig. 19. Although this calculation produces double peaks at forward angles, they do not resemble those seen in the data, and the disagreement with the large-angle cross sections becomes even greater than that seen in Fig. 19.

#### D. Intranuclear Cascade Calculation with Inclusion of Pion Production

Alqadi and Gibbs[40] have calculated doubly differential cross sections for  ${}^4\text{He}(\pi^+, \pi^-)$  using an intranuclear cascade (INC) code. Pions are allowed to propagate classically through the nucleus and interact with the nucleons via absorption, elastic scattering, charge exchange, or pion production processes as permitted by energy and charge conservation, with the relative interaction probabilities given by the ratio of the relevant cross sections to the total cross section. The effects of Pauli blocking and final state interactions are taken into account. Comparisons of the calculations with the present data at 240 and 270 MeV are shown in Ref. [40]; the results will be summarized here.

1. When only two nucleons (neutrons) are allowed to be active in the INC, the resulting  $(\pi^+, \pi^-)$  cross section is found to be very similar to that obtained using the two-nucleon SSCX model discussed in Sect. VII.A.<sup>4</sup>

2. Allowing all four nucleons to be active in the INC reduces the cross section by a factor of  $\sim 2$ , in better agreement with the data. The two protons, with their large cross section for elastic scattering of positive pions, effectively “shield” the neutrons from the incoming pions and thus reduce the probability of their initiating of a DCX reaction.<sup>5</sup>

3. Final state interactions, as in the two-nucleon model, mainly affect the cross section for outgoing pions at forward angles and high energies.

4. At 180 and 240 MeV, as one goes from forward to backward angles, the calculation goes from being slightly lower than the measured cross section (at  $25^\circ$  and  $50^\circ$ ) to being slightly larger (at  $105^\circ$ ) to being as much as a factor of two larger (at  $130^\circ$ ).<sup>6</sup> This angular dependence, though not as severe here, is reminiscent of that found in the non-static SSCX calculations described above.

5. At 240 and 270 MeV, the calculation with pion production “turned off” does not exhibit a double-peaked structure; the low-energy peak is absent. Inclusion of pion production adds strength to the low pion energy region, as expected, so that the resulting theoretical cross section is double-peaked, in fair agreement with the data at  $25^\circ$  and  $50^\circ$ .<sup>7</sup>

6. The calculation is unable to reproduce the double-peaked structure seen at  $25^\circ$  and

---

<sup>4</sup> See Fig. 2 in Ref. [40]

<sup>5</sup> See Fig. 3 in Ref. [40]

<sup>6</sup> See Figs. 4 and 6 in Ref. [40]

<sup>7</sup> See Figs. 7 and 8 in Ref. [40]

50° for incident energy 180 MeV.<sup>8</sup> The low-energy peak in this case cannot be attributed to pion production.

## VIII. SUMMARY AND CONCLUSIONS

The results of an experimental investigation of the pion double charge exchange (DCX) reaction in  ${}^4\text{He}$  at intermediate incident energies have been presented. Study of the reaction is motivated by interest in understanding the reaction of pions with the nucleus, particularly the role of multiple scattering in such reactions. Pion double charge exchange is an ideal probe of such processes because two nucleons must be involved in the reaction in order to conserve charge. Moreover, the intimate connection of the pion to the nuclear potential at long range makes an understanding of pion-nucleus reactions important to all attempts to investigate the structure and dynamics of the nucleus.

The measurements presented here constitute the first systematic investigation of the DCX reaction in  ${}^4\text{He}$  for a broad range of incident pion energies and outgoing pion angles. The doubly differential cross sections for the inclusive reaction  ${}^4\text{He}(\pi^+, \pi^-)4p$  have been measured at five incident pion energies in the range 120–270 MeV, and for the reaction  ${}^4\text{He}(\pi^-, \pi^+)4n$  at 180 and 240 MeV. At each incident energy, the cross sections were measured at from three to five angles between 25° and 130°, over the entire energy range of the outgoing pions above 10 MeV. The ability to detect low energy pions was particularly important in view of the large fraction of the yield which results from reactions leading to pions with energies below 50 MeV. The doubly differential cross sections have been integrated to obtain both angular distributions and total reaction cross sections.

An interesting feature of the DCX energy spectra measured at forward angles is a prominent peak at high outgoing pion energy, which changes in magnitude and energy as the scattering angle is increased; this feature was apparent in the spectra from both  ${}^4\text{He}(\pi^+, \pi^-)4p$  and  ${}^4\text{He}(\pi^-, \pi^+)4n$  reactions. Empirical analysis of the peak indicates that it does not arise from a resonant state of four nucleons or from a reaction with a “cluster” in the nucleus. The structure had not been observed in earlier measurements, primarily owing to the incomplete survey of the reactions carried out.

---

<sup>8</sup> See Fig. 6 in Ref. [40]

The results of several calculations of the DCX cross sections based on the sequential single charge exchange model of the reaction are presented. Although calculations employing the fixed-nucleon approximation[37, 38, 40] do not reproduce the data, a non-static SSCX calculation is able to account for many features of the measurements. In this model[10], the high energy peak is a manifestation of the basic  $p$ -wave character of the  $\pi N$  interaction near the energy of the  $\Delta$  resonance. Because forward and backward scattering are preferred relative to scattering at intermediate angles, forward double scattering consists mostly of two forward or two backward reactions. The energy losses of the pions in the two cases are quite different, however, and lead to high- and low-energy components of the outgoing pion spectrum at forward angles. In this calculation, all continuum states are treated as plane waves and precise agreement of the absolute magnitude of the theoretical predictions with the measured cross sections is therefore not expected. The shapes of the predicted energy spectra may be more meaningful. In particular, to reproduce the shape of the measured spectra, it was found to be important to treat the  $\pi N$  interaction non-statically so as to include the Fermi motion of the nucleons in the determination of the relative energy of the  $\pi N$  system. Sensitivity to the inclusion of the nuclear binding potential was also found.

An attempt[38] to remove some of the approximations in the above-mentioned calculation, by use of a relativistic three-body model of  $\pi$ -nuclear interactions, did not result in improved agreement with the data.

A recent intranuclear cascade calculation[40], with the inclusion of the pion-induced pion production (PIPP) process, provides good agreement with some of the data at 240 and 270 MeV. Without PIPP, the peak at low pion energies in the forward-angle data is missing. However, PIPP cannot be responsible for the low-energy forward-angle peaks seen at 180 MeV or at 150 MeV (well below threshold). We note that in the  ${}^3\text{He}(\pi^-, \pi^+)$  reaction[12], forward angle double peaks were seen at all incident energies at which measurements were made: 240, 180, and 120 MeV.

In summary, the calculations presented here are seen to reproduce some features of the measured cross sections. However, a more complete theoretical treatment is evidently required to account for the shapes, magnitudes, and incident pion energy dependence of the doubly differential, singly differential, and total reaction cross sections for inclusive DCX in  ${}^4\text{He}$ .



## IX. ACKNOWLEDGMENTS

This work was supported in part by funds provided by the U.S. Department of Energy. We would like to thank S. A. Wood for sharing his wisdom and experience in the analysis of the data, and W. R. Gibbs for making his code available for our perusal. One of us (ERK) wishes to acknowledge E. J. Moniz and M. Thies for their helpful discussions of the theory. We also wish to thank T. Akdoğan for his assistance in preparing the figures.

- 
- [1] R. E. P. Davis *et al.*, Bull. Amer. Phys. Soc. **9**,127 (1964).
  - [2] L. Gilly *et al.*, Phys. Lett. **19**, 335 (1965).
  - [3] L. Kaufman, V. Perez-Mendez, and J. Sperinde, Phys. Rev. **175**, 1358 (1968).
  - [4] J. E. Ungar *et al.*, Phys. Lett. **144B**, 333 (1984).
  - [5] N. Carayannopoulos, J. Head, N. Kwak, J. Manweiler, and R. Stump, Phys. Rev. Lett. **20**, 1215 (1968).
  - [6] F. Gaille *et al.*, Nuovo Cimento **40A**, 31 (1977).
  - [7] J.-B. Jeanneret, M. Bogdanski, and E. Jeannet, Nucl. Phys. **A350**, 345 (1980).
  - [8] I. V. Falomkin, M. M. Kulyukin, V. I. Lyashenko, G. B. Pontecorvo, Yu. A. Shcherbakov, C. Georgescu, A. Mihul, F. Nichitu, A. Sararu, and G. Piragino, Nuovo Cimento A **22**, 333 (1974).
  - [9] I. V. Falomkin *et al.*, Lett. Nuovo Cimento **16**, 525 (1976).
  - [10] E. R. Kinney, Los Alamos National Laboratory Report No. LA-11417-T, 1988.
  - [11] S. A. Wood, J. L. Matthews, E. R. Kinney, P. A. M. Gram, G. A. Rebka, Jr., and D. A. Roberts, Phys. Rev. C **46**, 1903 (1992).
  - [12] M. Yuly, W. Fong, E. R. Kinney, C. J. Maher, J. L. Matthews, T. Soos, J. Vail, M. Y. Wang, S. A. Wood, P. A. M. Gram, G. A. Rebka, Jr. and D. A. Roberts, Phys. Rev. C **55**, 1848 (1997).
  - [13] R. E. Mischke, A. Blomberg, P. A. M. Gram, J. Jansen, J. Zichy, J. Bolger, E. Boschitz, C. H. Q. Ingram, and G. Pröbstle, Phys. Rev. Lett. **44**, 1197 (1980).
  - [14] A. Stetz *et al.*, Phys. Rev. Lett. **47**, 782 (1981).
  - [15] A. Stetz *et al.*, Nucl. Phys. **A457**, 669 (1986).

- [16] J. Gräter *et al.*, Phys. Rev. C **58**, 1576 (1998).
- [17] J. Sperinde, D. Fredrickson, R. Hinkins, V. Perez-Mendez, and B. Smith, Phys. Lett. B **32**, 185 (1970); J. Sperinde, D. Fredrickson, and V. Perez-Mendez, Nucl. Phys. **B78**, 345 (1974).
- [18] F. Becker and C. Schmit, Nucl. Phys. **B18**, 607 (1970).
- [19] F. Becker and Z. Marić, Nuovo Cimento **36**, 1395 (1965), **41**, 174 (1966).
- [20] F. Becker and Yu. A. Batusov, Riv. Nuovo Cimento **1**, 309 (1971).
- [21] J.-F. Germond and C. Wilkin, Lett. Nuovo Cimento **13**, 605 (1975).
- [22] J.-F. Germond and C. Wilkin, in *Mesons in Nuclei*, edited by M. Rho and D. Wilkinson (North-Holland Publishing Company, Amsterdam, 1979), p.439.
- [23] S. Weinberg, Phys. Rev. Lett **17**, 616 (1966)
- [24] J. D. Bjorken and S. D. Drell, *Relativistic Quantum Mechanics*, McGraw-Hill Book Company, New York, 1964.
- [25] M. R. Robilotta and C. Wilkin, J. Phys. G. (Nucl. Phys.) **4**, L115 (1978).
- [26] W. R. Gibbs, B. F. Gibson, A. T. Hess, and G. J. Stephenson, Jr., Phys. Rev. **C15**, 1384 (1977).
- [27] W. R. Gibbs, Phys. Rev. C **3**, 1127 (1971); W. R. Gibbs, A. T. Hess, and W. B. Kaufmann, Phys Rev. C **13**, 1982 (1976); W. R. Gibbs, in *NATO Advanced Study Institute on Theoretical Methods in Intermediate Energy and Heavy Ion Physics, Madison, 1978*, edited by K. W. McVoy and W. Freedman, Plenum Press, New York, 1979, p. 503; W. R. Gibbs, B. F. Gibson, A. T. Hess, G. J. Stephenson, Jr., and W. B. Kaufmann, Phys. Rev. C **13**, 2433 (1976); W. B. Kaufmann, J. C. Jackson, and W. R. Gibbs, Phys. Rev. C **9**, 1340 (1974).
- [28] R. I. Dzhibuti, R. Ya. Kezerashvili, and K. I. Sigua, Sov. J. Nucl. Phys. **32**, 795 (1980).
- [29] R. I. Jibuti, R. Ya. Kezerashvili, and K. I. Sigua, Phys. Lett. B **102**, 381 (1981);
- [30] R. I. Dzhibuti and R. Ya. Kezerashvili, Yad. Fiz. **39**, 419 (1984) [Sov. J. Nucl. Phys. **39**, 264 (1984)]
- [31] R. I. Jibuti and R. Ya. Kezerashvili, Nucl. Phys. **A437**, 687 (1985).
- [32] R. I. Dzhibuti and R. Ya. Kezerashvili, Fiz. Elem. Chastits At. Yadra **16**, 1173 (1985) [Sov. J. Part. Nucl. **16**, 519 (1986)].
- [33] R. Ya. Kezerashvili, Yad. Fiz. **44**, 842 (1986) [Sov. J. Nucl. Phys. **44**, 542 (1987)].
- [34] J. Hüfner and M. Thies, Phys. Rev. C **20**, 273 (1979).
- [35] E. Oset, L. L. Salcedo, and D. Strottman, Phys. Lett. B **165**, 13 (1985); E. Oset, in *Proc.*

- LAMPF Workshop on Pion Double Charge Exchange*, Los Alamos, 1985, Los Alamos National Laboratory report LA-10550-C; L. L. Salcedo, E. Oset, M. J. Vicente-Vacas, and C. García-Recio Nucl. Phys. **A484**, 557 (1988); M. J. Vicente, E. Oset, L. L. Salcedo, and C. García-Recio, Phys. Rev. C **39**, 209 (1989); M. Vicente-Vacas and E. Oset, in *Second LAMPF International Workshop on Pion-Nucleus Double Charge Exchange*, Los Alamos, 1989, edited by W. R. Gibbs and M. J. Leitch (World Scientific, Singapore, 1990), p. 120.
- [36] W. Fong, Ph.D. Thesis, Massachusetts Institute of Technology, 1994; W. Fong *et al.*, to be published.
- [37] G. A. Rebka, Jr., private communication.
- [38] A. V. Kulkarni, Ph.D. Dissertation, University of Wyoming, 1994, unpublished.
- [39] G. Rowe, M. Salomon, and R. H. Landau, Phys. Rev. C **18**, 584 (1978).
- [40] M. Alqadi and W. R. Gibbs, Phys. Rev. C **65**, 044609 (2002).
- [41] E. R. Kinney, J. L. Matthews, P. A. M. Gram, D. W. MacArthur, E. Piasetzky, G. A. Rebka, Jr., and D. A. Roberts, Phys. Rev. Lett. **57**, 3152 (1986).
- [42] J. B. Walter and G. A. Rebka, Jr., Los Alamos National Laboratory Technical Report No. LA-7731-MS (1979).
- [43] D. C. Carey, K. L. Brown, and Ch. Iselin, Stanford Linear Accelerator Center Report No. SLAC-246, 1982.
- [44] S. A. Wood, Los Alamos National Laboratory Report No. LA-9932-T, 1983.
- [45] E. Piasetzky, P. A. M. Gram, D. W. MacArthur, G. A. Rebka, Jr., C. A. Bordner, S. Høibråten, E. R. Kinney, J. L. Matthews, S. A. Wood, D. Ashery, and J. Lichtenstadt, Phys. Rev. Lett. **53**, 540 (1984); J. Lichtenstadt, D. Ashery, S. A. Wood, E. Piasetzky, P. A. M. Gram, D. W. MacArthur, R. S. Bhalerao, L. C. Liu, G. A. Rebka, Jr. and D. Roberts, Phys. Rev. C **33**, 655 (1986).
- [46] N. Grion *et al.*, Phys. Rev. Lett. **59**, 1080 (1987).
- [47] P. A. M. Gram, S. A. Wood, E. R. Kinney, S. Høibråten, P. Mansky, J. L. Matthews, T. Soos, G. A. Rebka, Jr., and D. A. Roberts, Phys. Rev. Lett. **62**, 1837 (1989).
- [48] R. D. McKeown *et al.*, Phys. Rev. Lett. **44**, 1033 (1980)
- [49] R. A. Schumacher, G. S. Adams, D. R. Ingham, J. L. Matthews, W. W. Sapp, R. S. Turley, R. O. Owens, and B. L. Roberts, Phys. Rev. C **25**, 2269 (1982).
- [50] P. Weber *et al.*, Nucl. Phys. **A534**, 541 (1991); T. Altholz *et al.*, Phys. Rev. Lett. **73**, 1336

- (1994); A. O. Mateos *et al.*, Phys. Rev. C **58**, 942 (1998).
- [51] C. W. Bjork *et al.*, Phys. Rev. Lett. **44**, 62 (1980).
- [52] G. Kernel *et al.*, Phys. Lett. **B216**, 244 (1989).
- [53] H. Burkhardt and J. Lowe, Phys. Rev. Lett. **67**, 2622 (1991).
- [54] M. Thies, private communication.
- [55] J. van Loon, Master's Thesis, Free University, Amsterdam, 1985.
- [56] M. Thies, Ann. Phys. (N. Y.) **123**, 411 (1979).
- [57] E. R. Kinney, to be published.
- [58] F. Lenz, Ann. Phys. (N. Y.) **95**, 348 (1975).
- [59] M. Hirata, J. H. Koch, F. Lenz, and E. J. Moniz, Ann. Phys. (N.Y.) **120**, 205 (1979).
- [60] M. Hirata, F. Lenz, and K. Yazaki, Ann. Phys. (N.Y.) **108**, 116 (1977).
- [61] M. Thies, Nucl. Phys. **A382**, 434 (1982).
- [62] M. Baumgartner, H. P. Gubler, G. R. Plattner, W. D. Ramsay, H. W. Roser, I. Sick, P. Zupranski, J. P. Egger, and M. Thies, Nucl. Phys. **A399**, 451 (1983).
- [63] R. F. Frosch, J. S. McCarthy, R. E. Rand, and M. R. Yearian, Phys. Rev. **160**, 874 (1967).
- [64] R. A. Arndt, Z. Li, L. D. Roper, R. L. Workman, and J. M. Ford, Phys. Rev. D **43**, 2131 (1991).
- [65] F. Lenz, M. Thies, and Y. Horikawa, Ann. Phys. (N. Y.) **120**, 266 (1982).
- [66] H. Garcilazo and W. R. Gibbs, Nucl. Phys. **A356**, 284 (1981).

TABLE I: Systematic uncertainties in the experiment.

| Systematic uncertainties (%) |                     |                   |       |                      |
|------------------------------|---------------------|-------------------|-------|----------------------|
| Incident Beam                | Angle Dependent     |                   |       | Overall <sup>c</sup> |
|                              | Thick. <sup>a</sup> | I.C. <sup>b</sup> | Total |                      |
| 120 MeV $\pi^+$              | 5.2                 | 1.0               | 5.3   | 5.7                  |
| 150 MeV $\pi^+$              | 5.5                 | 1.0               | 5.6   | 6.1                  |
| 180 MeV $\pi^+$              | 2.4                 | 1.0               | 2.6   | 3.6                  |
| 180 MeV $\pi^-$              | 4.7                 | 2.0               | 5.1   | 5.7                  |
| 240 MeV $\pi^+$              | 2.3                 | 1.0               | 2.5   | 3.5                  |
| 240 MeV $\pi^-$              | 7.4                 | 1.5               | 7.6   | 8.0                  |
| 270 MeV $\pi^+$              | 7.7                 | 1.5               | 7.8   | 8.2                  |

<sup>a</sup>Uncertainty in target thickness due to possible misalignment (see text).

<sup>b</sup>Normalization uncertainty due to variation in ionization chamber response (see text).

<sup>c</sup>Includes angle dependent and normalization uncertainties only. The uncertainties which depend on the energy of observation are included along with the statistical uncertainties in the plotted error bars.

TABLE II: Total reaction cross sections for  ${}^4\text{He}(\pi^+, \pi^-)$  and  ${}^4\text{He}(\pi^-, \pi^+)$ , and estimated cross sections for pion-induced pion production (see text).

| Reaction cross sections ( $\mu\text{b}$ ) |                       |                        |                                       |                       |
|---|-----------------------|------------------------|---------------------------------------|-----------------------|
| Incident Beam                             | $\sigma_{\text{tot}}$ | $\sigma_{\text{PIPP}}$ | $\sigma_{\text{PIPP}}({}^3\text{He})$ | $\sigma_{\text{DCX}}$ |
| 120 MeV $\pi^+$                           | $128 \pm 13$          |                        |                                       |                       |
| 150 MeV $\pi^+$                           | $280 \pm 18$          |                        |                                       |                       |
| 180 MeV $\pi^+$                           | $489 \pm 23$          | $2 \pm 1$              |                                       |                       |
| 180 MeV $\pi^-$                           | $418 \pm 25$          | $2 \pm 1$              |                                       |                       |
| 240 MeV $\pi^+$                           | $1014 \pm 36$         | $128 \pm 8$            | $90 \pm 20$                           | $886 \pm 138$         |
| 240 MeV $\pi^-$                           | $1075 \pm 76$         | $149 \pm 15$           |                                       | $926 \pm 77$          |
| 270 MeV $\pi^+$                           | $1460 \pm 105$        | $509 \pm 50$           |                                       | $951 \pm 116$         |

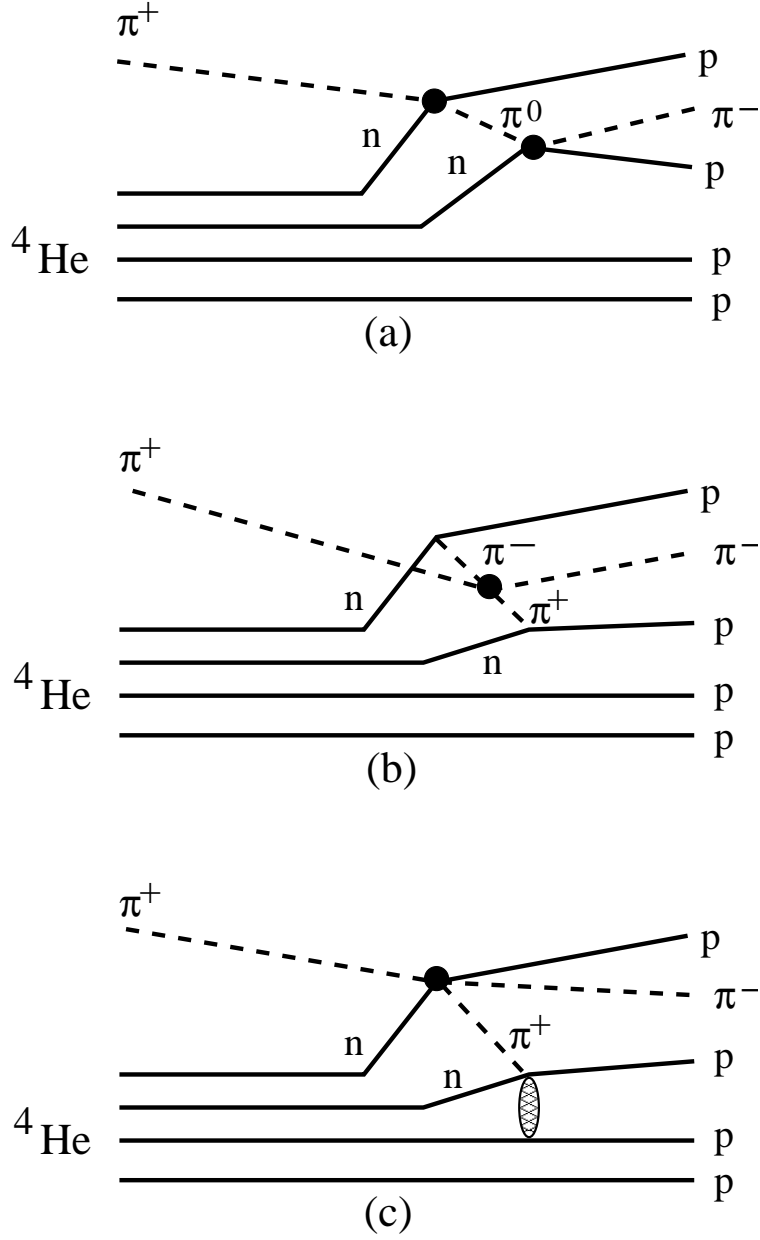


FIG. 1: Schematic diagram of (a) the SSCX mechanism, (b) the meson-exchange mechanism of Germond and Wilkin [21], and (c) the  $pn$  absorption mechanism of Jeanneret *et al.* [7] for the  ${}^4\text{He}(\pi^+, \pi^-)4p$  reaction.

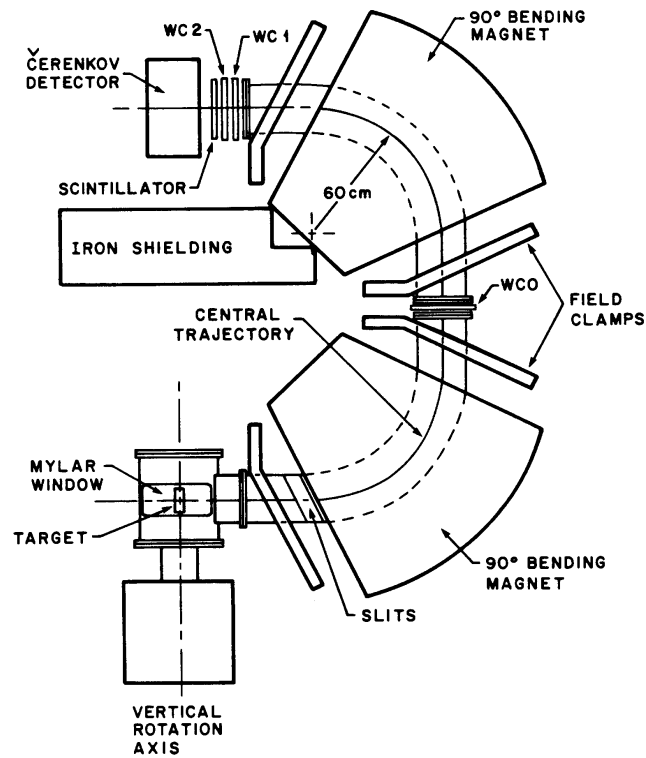


FIG. 2: Drawing of the  $180^\circ$  vertical bend, double focussing magnetic spectrometer. Pions travel through vacuum from the target, through two  $90^\circ$  dipole magnets, to the focal plane. There is a 2.5 cm break in the vacuum for WC0, the mid-spectrometer wire chamber, which is used to ensure that a particle traverses the entire spectrometer. Particle trajectories are traced back to the focal plane using information from two wire chambers, WC1 and WC2. The scintillator is used to distinguish positive pions from protons, as well as to provide time-of-flight information. The Čerenkov detector separates pions from electrons and positrons. The liquid  $^4\text{He}$  cryostat is not shown.

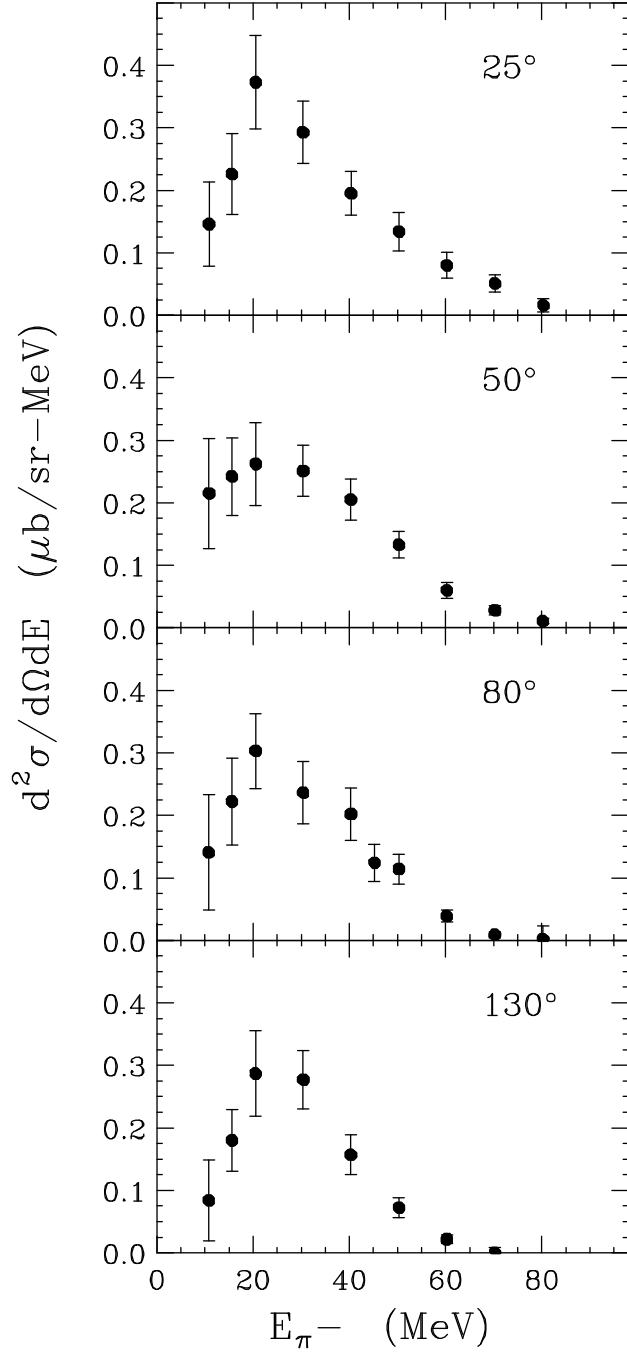


FIG. 3: Doubly differential cross sections for  ${}^4\text{He}(\pi^+, \pi^-)$  at 120 MeV for laboratory angles  $25^\circ$ ,  $50^\circ$ ,  $80^\circ$ , and  $130^\circ$ . The uncertainties shown include the statistical uncertainty and the systematic uncertainties which depend on the outgoing pion energy.



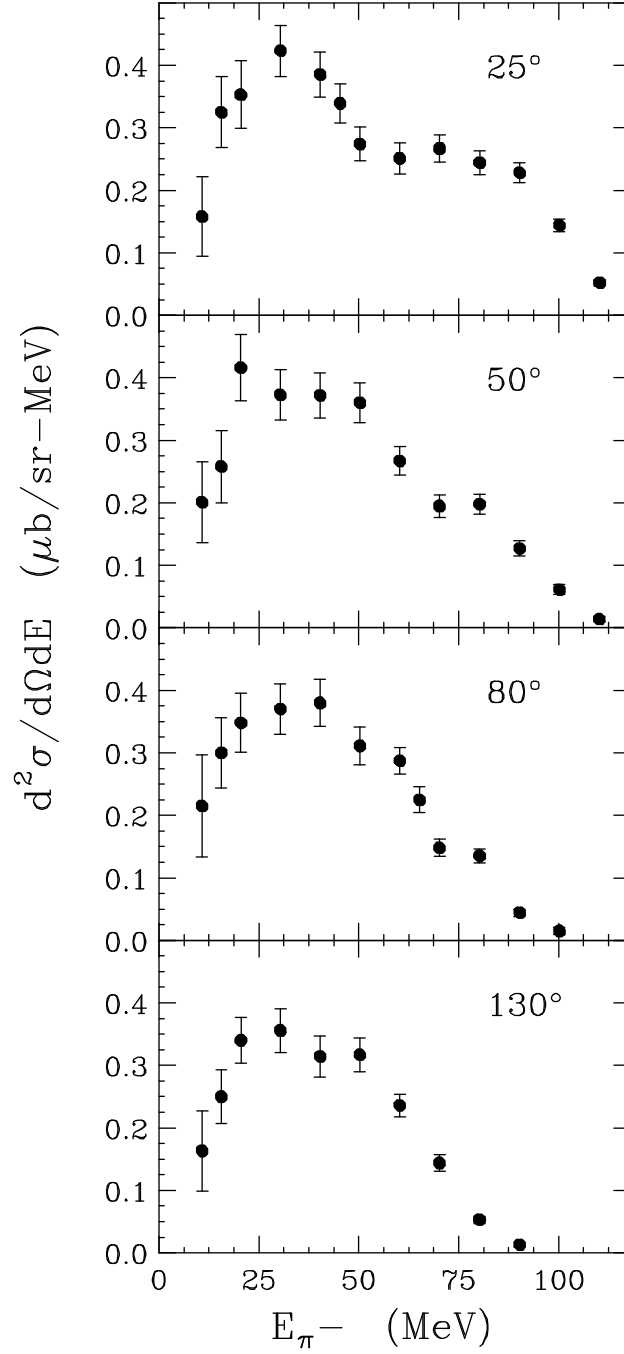


FIG. 4: Doubly differential cross sections for  ${}^4\text{He}(\pi^+, \pi^-)$  at 150 MeV for laboratory angles  $25^\circ$ ,  $50^\circ$ ,  $80^\circ$ , and  $130^\circ$ . The uncertainties shown include the statistical uncertainty and the systematic uncertainties which depend on the outgoing pion energy.

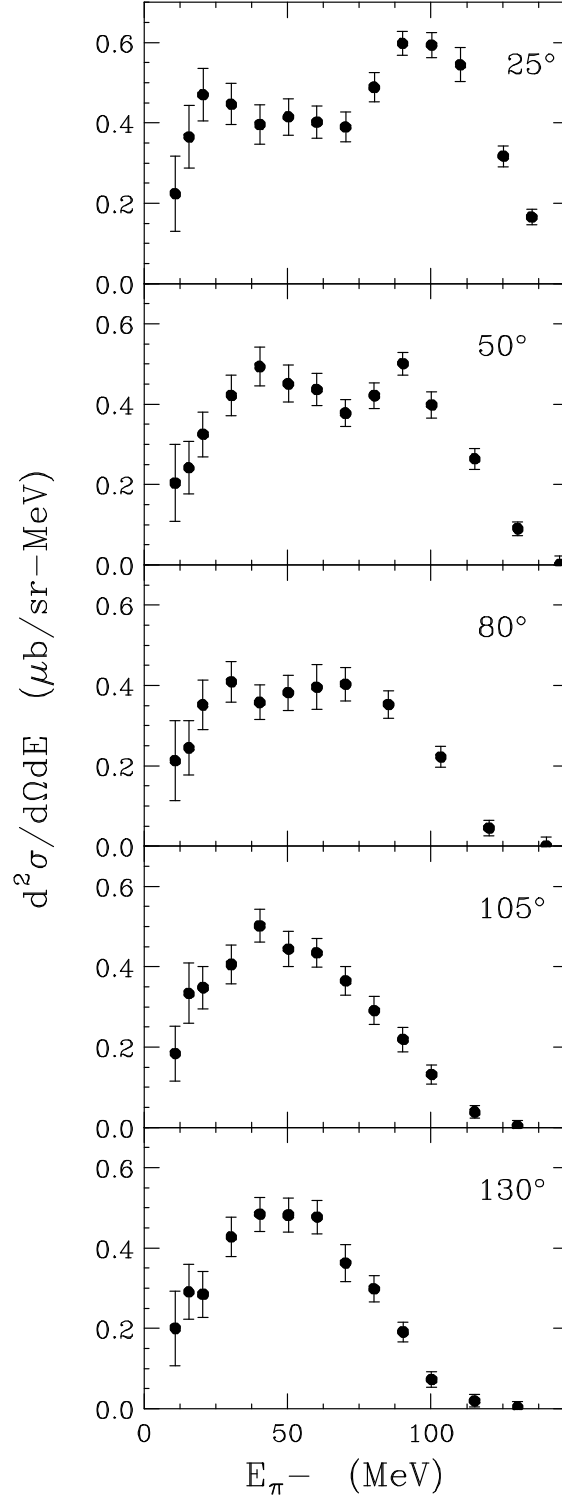


FIG. 5: Doubly differential cross sections for  ${}^4\text{He}(\pi^+, \pi^-)$  at 180 MeV for laboratory angles  $25^\circ$ ,  $50^\circ$ ,  $80^\circ$ ,  $105^\circ$ , and  $130^\circ$ . The uncertainties shown include the statistical uncertainty and the systematic uncertainties which depend on the outgoing pion energy.

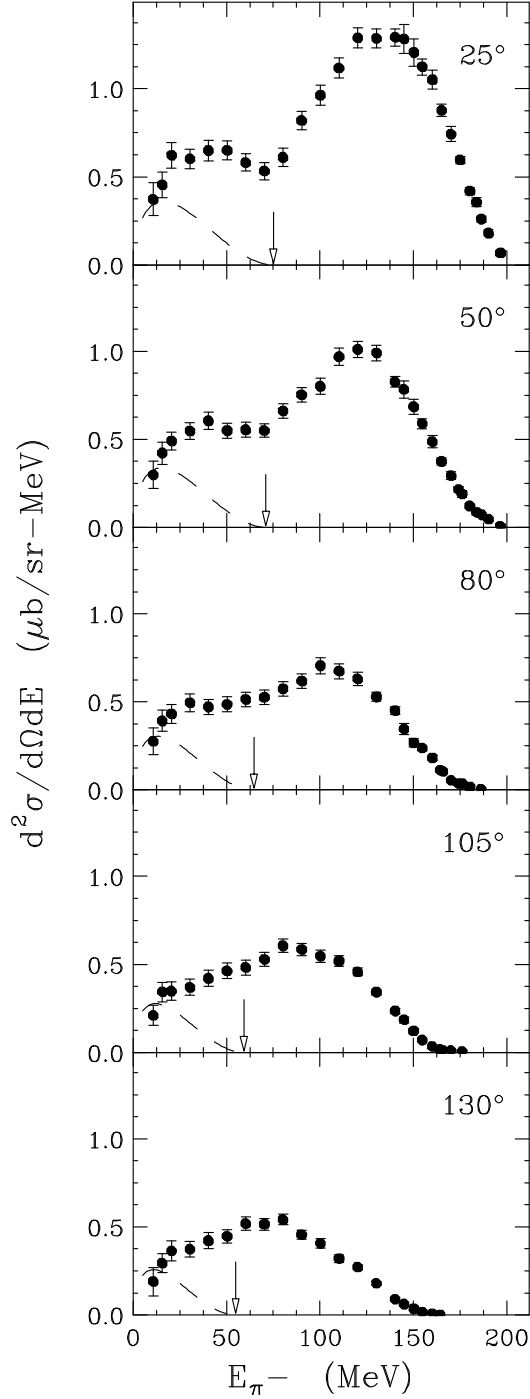


FIG. 6: Doubly differential cross sections for  ${}^4\text{He}(\pi^+, \pi^-)$  at 240 MeV for laboratory angles  $25^\circ$ ,  $50^\circ$ ,  $80^\circ$ ,  $105^\circ$ , and  $130^\circ$ . The uncertainties shown include the statistical uncertainty and the systematic uncertainties which depend on the outgoing pion energy. The arrow indicates the upper limit of outgoing pion energy from the pion-induced pion production process. The dashed curve represents the shape of the available phase space for pion production.

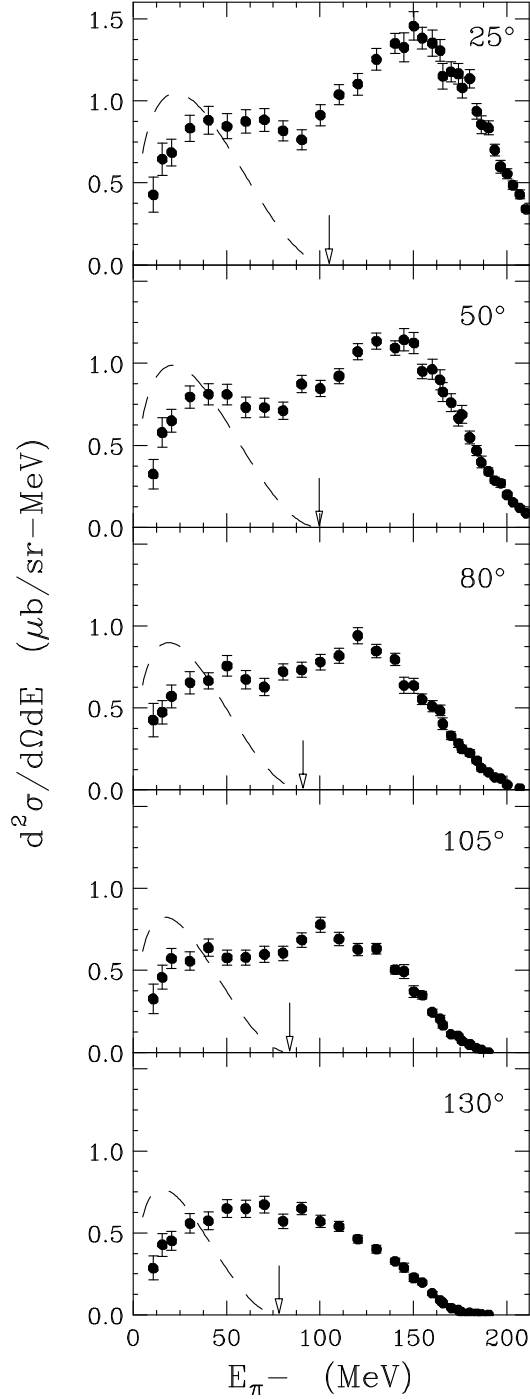


FIG. 7: Doubly differential cross sections for  ${}^4\text{He}(\pi^+, \pi^-)$  at 270 MeV for laboratory angles  $25^\circ$ ,  $50^\circ$ ,  $80^\circ$ ,  $105^\circ$ , and  $130^\circ$ . The uncertainties shown include the statistical uncertainty and the systematic uncertainties which depend on the outgoing pion energy. The arrow indicates the upper limit of outgoing pion energy from the pion-induced pion production process. The dashed curve represents the shape of the available phase space for pion production.

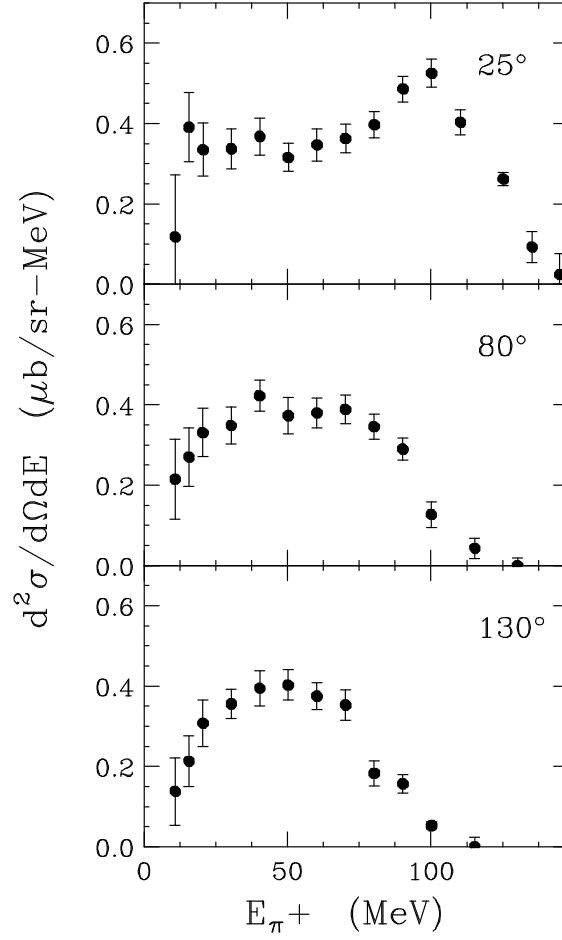


FIG. 8: Doubly differential cross sections for  ${}^4\text{He}(\pi^-, \pi^+)$  at incident pion energy 180 MeV for laboratory angles  $25^\circ$ ,  $80^\circ$ , and  $130^\circ$ . The uncertainties shown include the statistical uncertainty and the systematic uncertainties which depend on the outgoing pion energy.

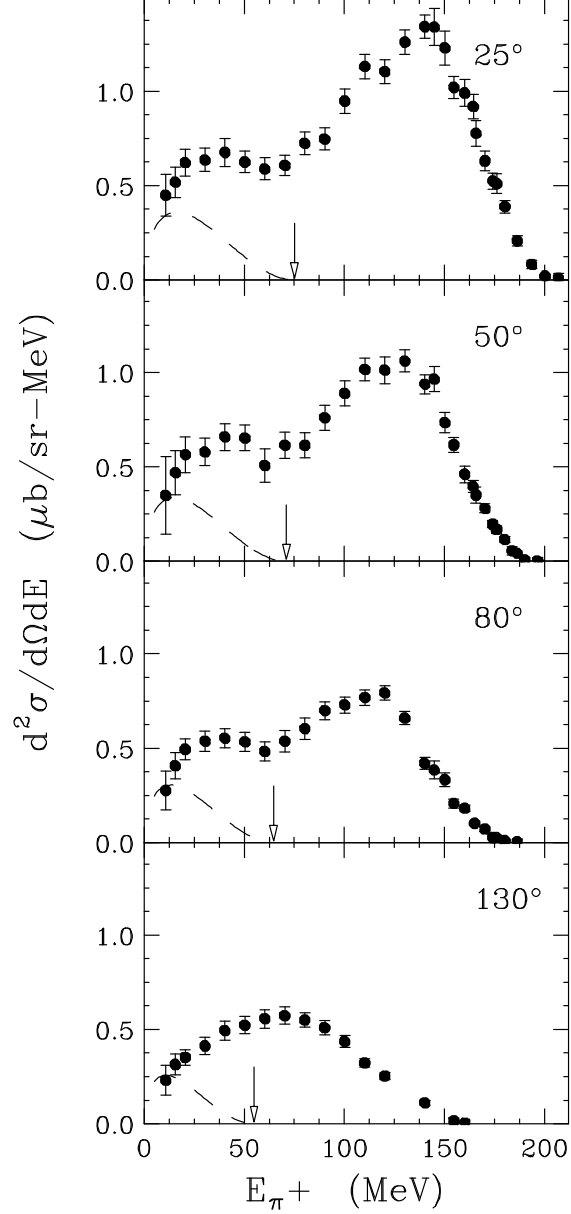


FIG. 9: Doubly differential cross sections for  ${}^4\text{He}(\pi^-, \pi^+)$  at incident pion energy 240 MeV for laboratory angles  $25^\circ$ ,  $50^\circ$ ,  $80^\circ$ , and  $130^\circ$ . The uncertainties shown include the statistical uncertainty and the systematic uncertainties which depend on the outgoing pion energy. The arrow indicates the upper limit of outgoing pion energy from the pion-induced pion production process. The dashed curve represents the shape of the available phase space for pion production.

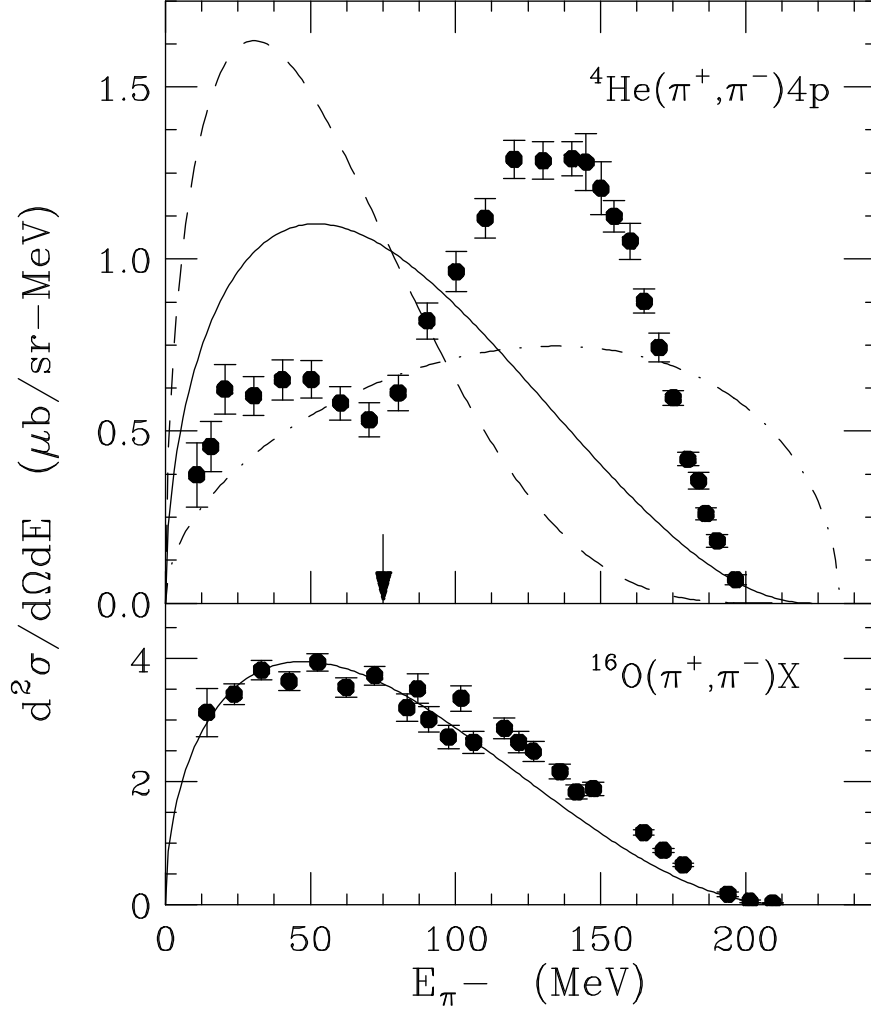


FIG. 10: A comparison of the doubly differential cross sections at 240 MeV and  $25^\circ$  for the  $(\pi^+, \pi^-)$  reactions in  ${}^4\text{He}$  and  ${}^{16}\text{O}$ . The  ${}^{16}\text{O}$  data are taken from Ref. [11]. The dashed and dot-dashed curves correspond to the distribution of events in five-body and three-body phase space, respectively, while the solid curves correspond to four-body phase space. The arrow indicates the maximum pion energy allowed in PIPP. The phase space curves are normalized as described in the text.

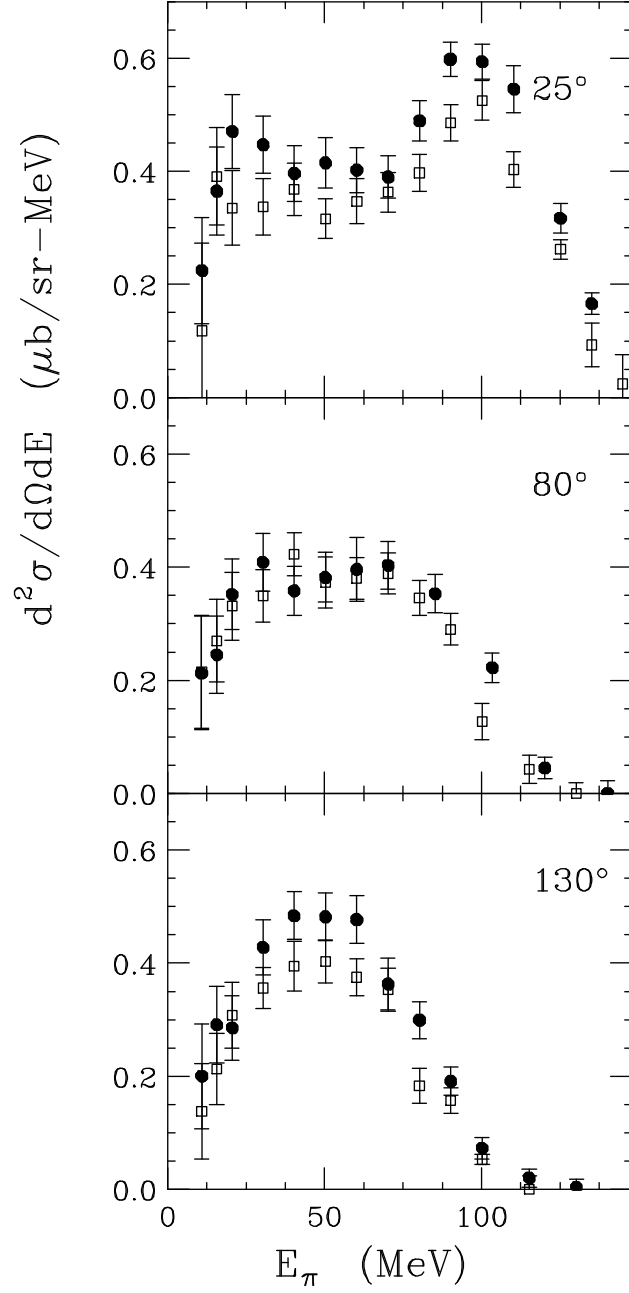


FIG. 11: A comparison of the doubly differential cross sections for  ${}^4\text{He}(\pi^+, \pi^-)$  (solid circles) and  ${}^4\text{He}(\pi^-, \pi^+)$  (open squares) at 180 MeV.



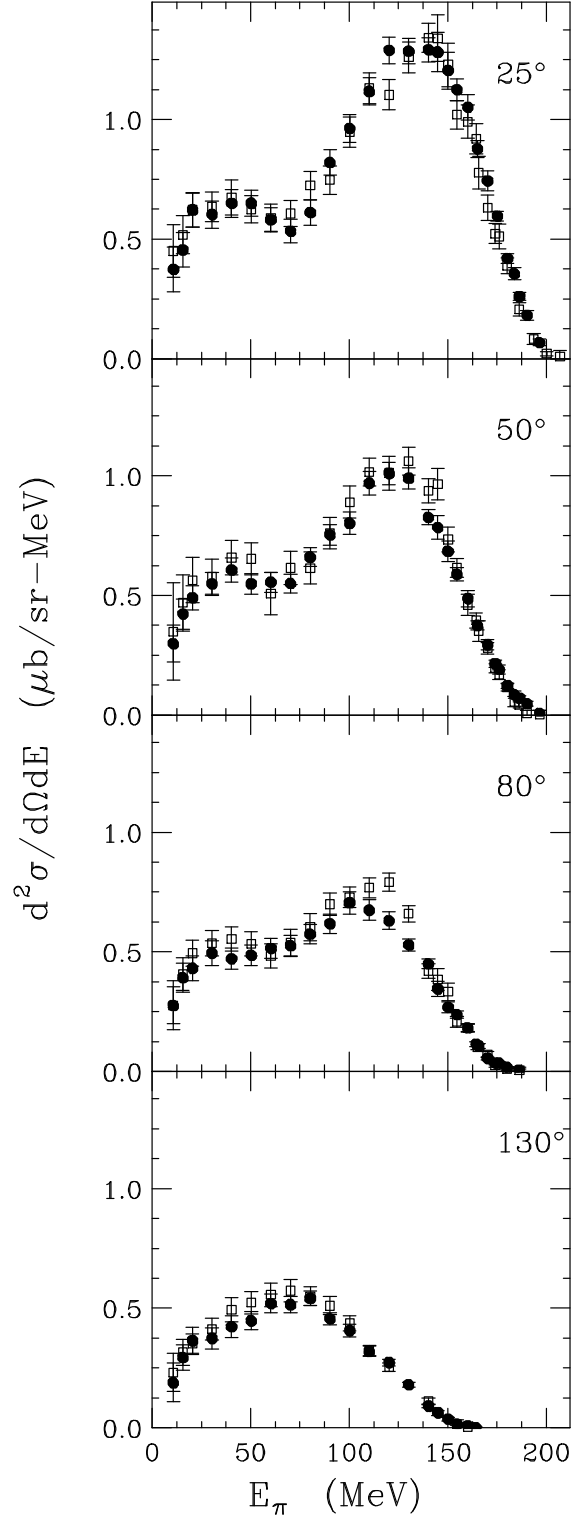


FIG. 12: A comparison of the doubly differential cross sections for  ${}^4\text{He}(\pi^+, \pi^-)$  (solid circles) and  ${}^4\text{He}(\pi^-, \pi^+)$  (open squares) at 240 MeV.

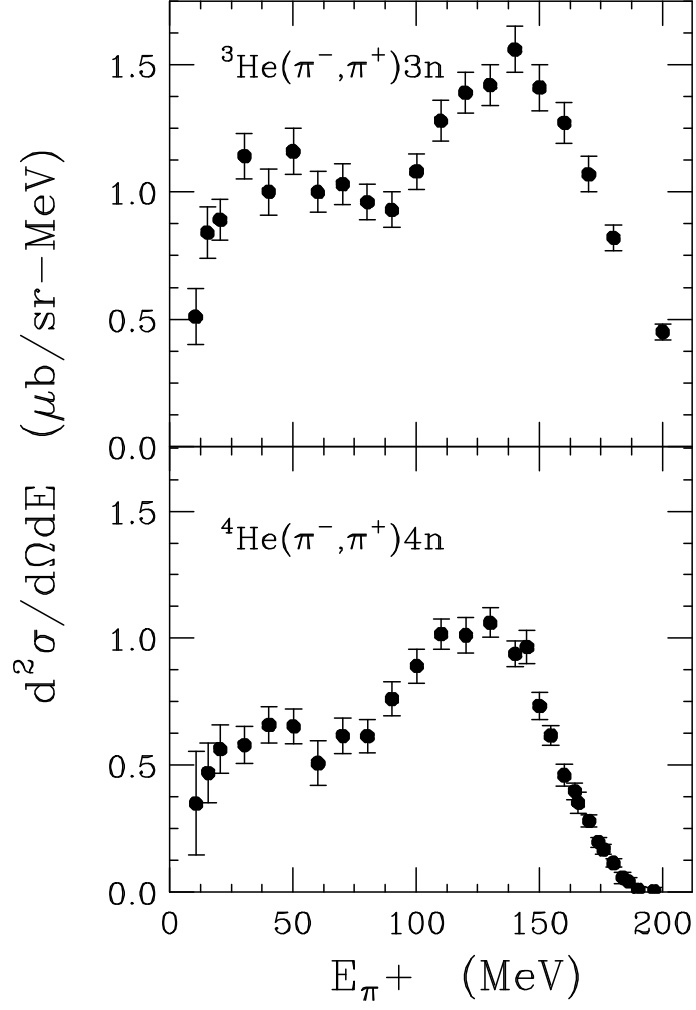


FIG. 13: A comparison of the doubly differential cross sections for  ${}^3\text{He}(\pi^-, \pi^+)$  and  ${}^4\text{He}(\pi^-, \pi^+)$  at 240 MeV and  $50^\circ$ .

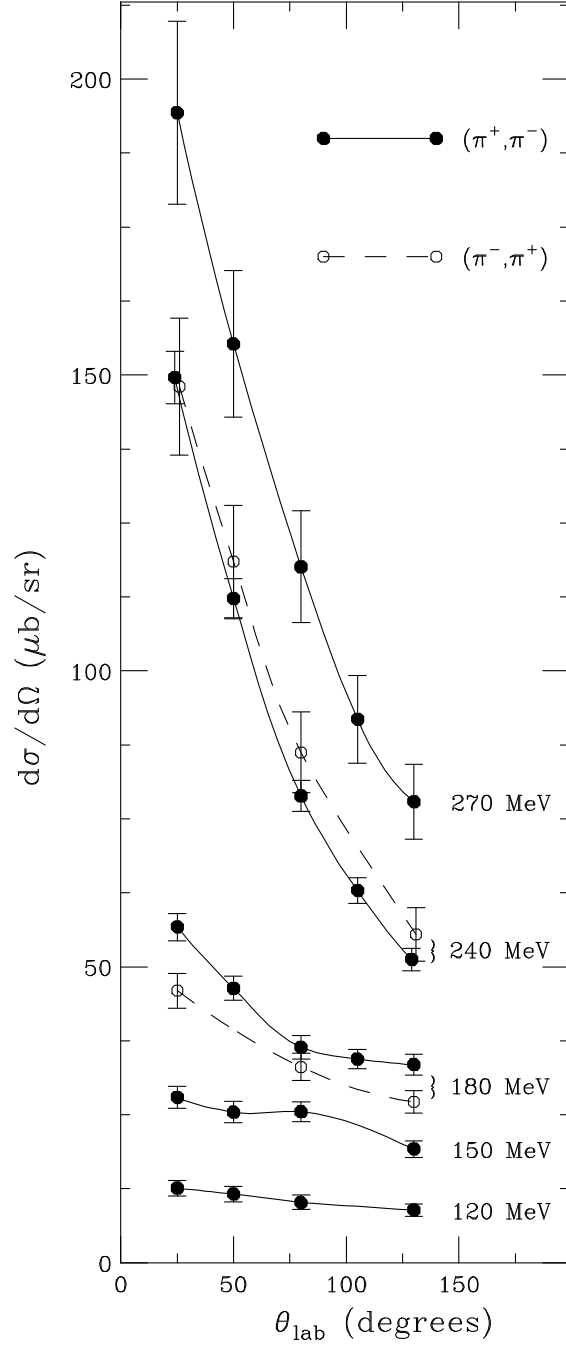


FIG. 14: Angular distributions for  ${}^4\text{He}(\pi^+, \pi^-)$  (solid circles) and  ${}^4\text{He}(\pi^-, \pi^+)$  (open circles) at 120, 150, 180, 240, and 270 MeV. The uncertainties indicated include the statistical uncertainty, the uncertainties arising from the extrapolation and integration procedure (see Sect. V.G), and the systematic uncertainties which depend on the outgoing pion energy and angle. The curves serve only to guide the eye.

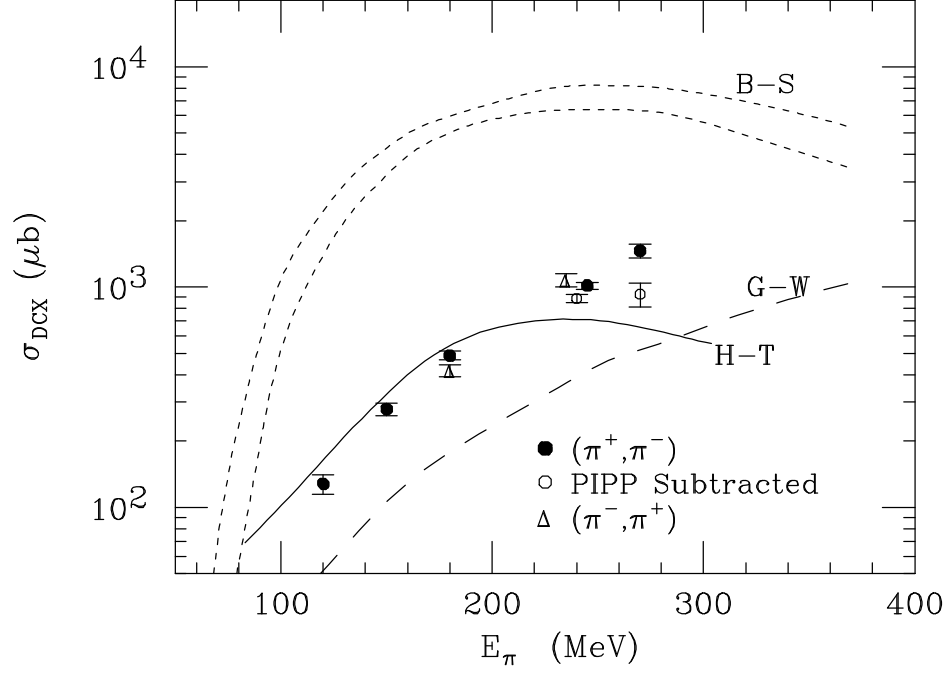


FIG. 15: Total reaction cross sections for  ${}^4\text{He}(\pi^+, \pi^-)$  (solid circles) and  ${}^4\text{He}(\pi^-, \pi^+)$  (open triangles) as a function of incident pion energy. The open circles are the  $(\pi^+, \pi^-)$  cross sections at 240 MeV and 270 MeV after subtraction of the estimated contribution of pion-induced pion production. The curves represent theoretical predictions which are discussed in the text.

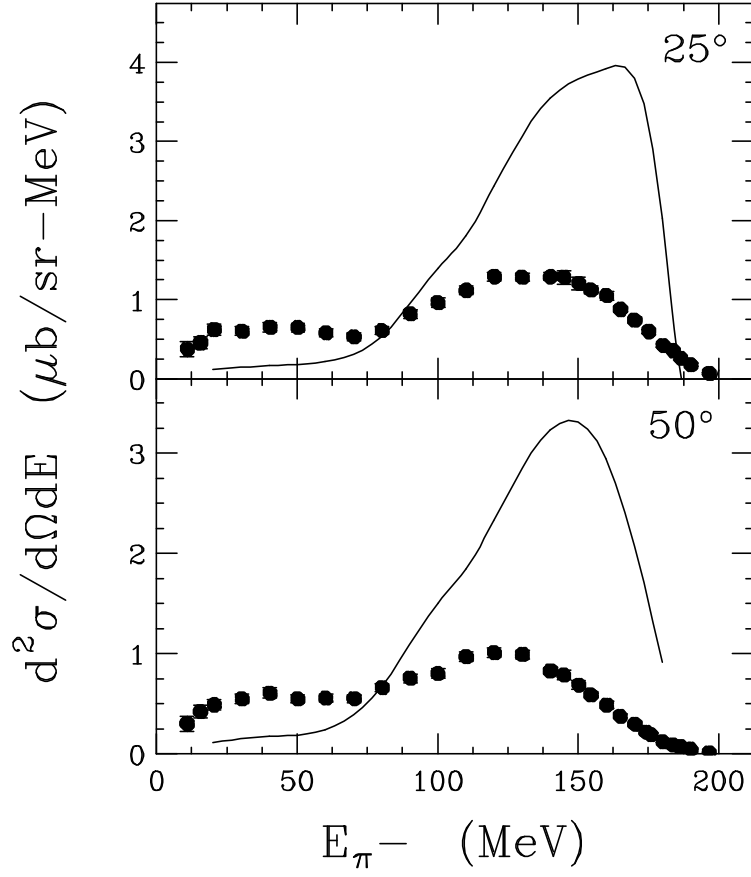


FIG. 16: Comparison of the calculation of Rebka and Kulkarni[37, 38], based on the fixed-nucleon calculation of Gibbs *et al.*[26], with the  ${}^4\text{He}(\pi^+, \pi^-)$  cross sections at incident energy 240 MeV and laboratory angles  $25^\circ$  and  $50^\circ$ .

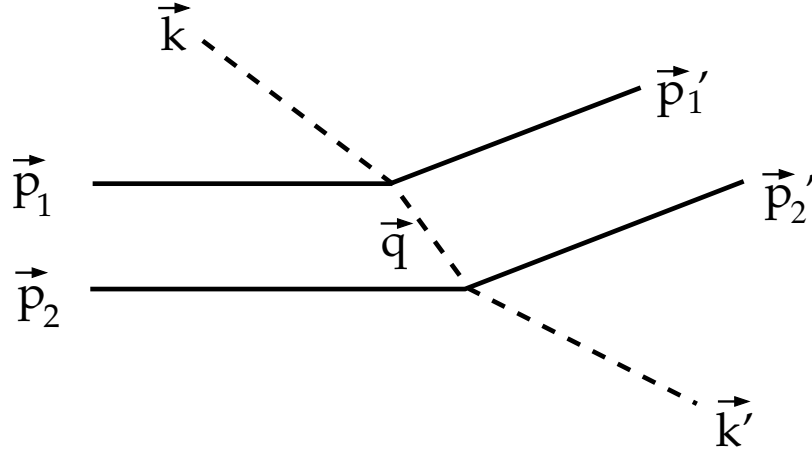


FIG. 17: Diagram of the SSCX process showing the intermediate pion momentum  $\vec{q}$  and the incident and knocked-out nucleon momenta  $\vec{p}_1$ ,  $\vec{p}_2$ ,  $\vec{p}'_1$ , and  $\vec{p}'_2$ .

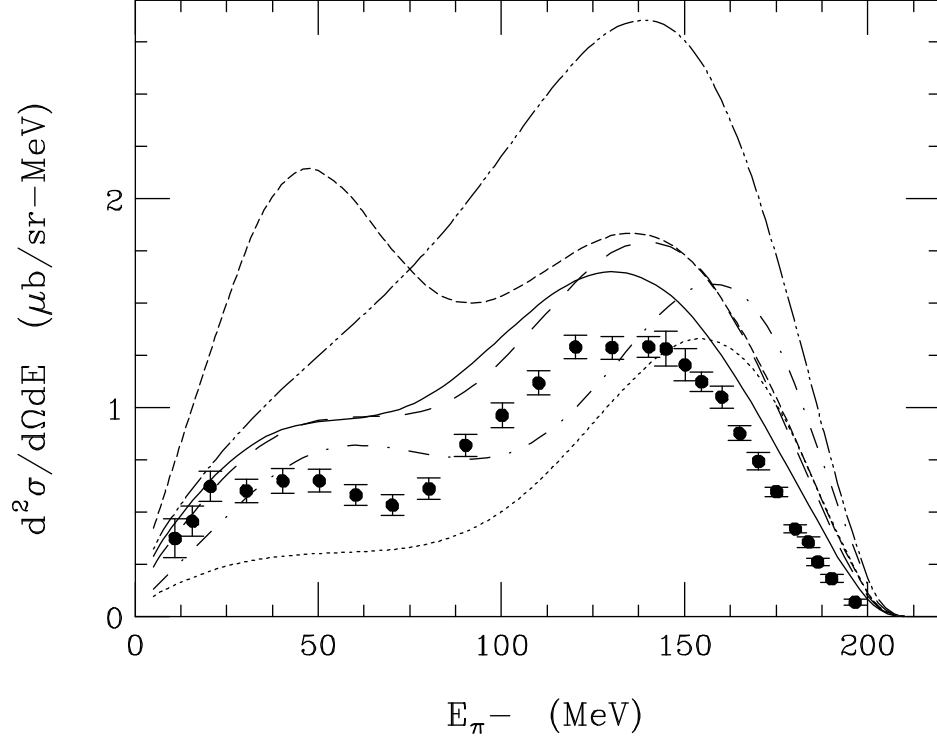


FIG. 18: Doubly differential cross section for  ${}^4\text{He}(\pi^+, \pi^-)$  at 240 MeV and  $25^\circ$  in comparison with predictions of the non-static sequential single charge exchange model. The curves represent different assumptions for the nuclear potentials in the first and second scattering (see text):  $U_1 = U_2 = -55$  MeV (solid curve);  $U_1 = U_2 = -37$  MeV (long-dashed curve);  $U_1 = U_2 = 0$  (dot-dashed curve);  $U_1 = -55$  MeV,  $U_2 = 0$  (dotted curve);  $U_1 = 0$ ,  $U_2 = -55$  MeV (short-dashed curve). The double-dot-dashed curve represents the static prescription (nucleons at rest) with  $U_1 = U_2 = 0$ .

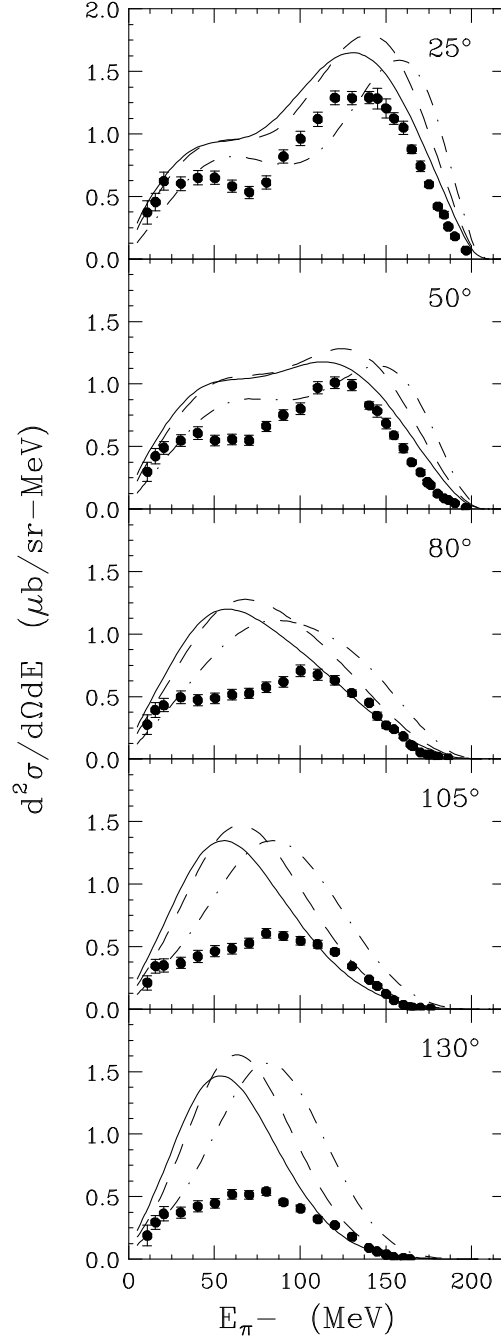


FIG. 19: Doubly differential cross sections for  ${}^4\text{He}(\pi^+, \pi^-)$  at 240 MeV and laboratory angles  $25^\circ$ ,  $50^\circ$ ,  $80^\circ$ ,  $105^\circ$ , and  $130^\circ$ . The theoretical curves are the same as in Fig. 18 using the average nuclear potentials  $U_1 = U_2 = -55$  MeV (solid curve),  $U_1 = U_2 = -37$  MeV (dashed curve), and  $U_1 = U_2 = 0$  (dot-dashed curve).



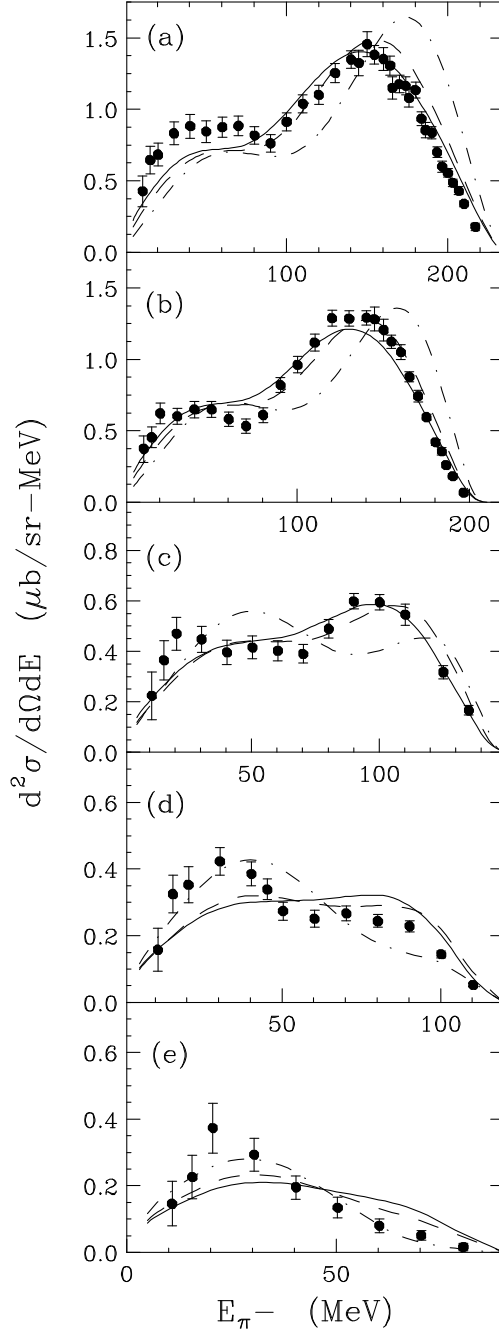


FIG. 20: Doubly differential cross sections for  ${}^4\text{He}(\pi^+, \pi^-)$  at laboratory angle  $25^\circ$  for incident energies 270 (a), 240 (b), 180 (c), 150 (d), and 120 (e) MeV, using the average nuclear potentials  $U_1 = U_2 = -55$  MeV (solid curve),  $U_1 = U_2 = -37$  MeV (dashed curve), and  $U_1 = U_2 = 0$  (dot-dashed curve). The theoretical predictions have been normalized to yield the same integrated areas as those of the measured cross sections.

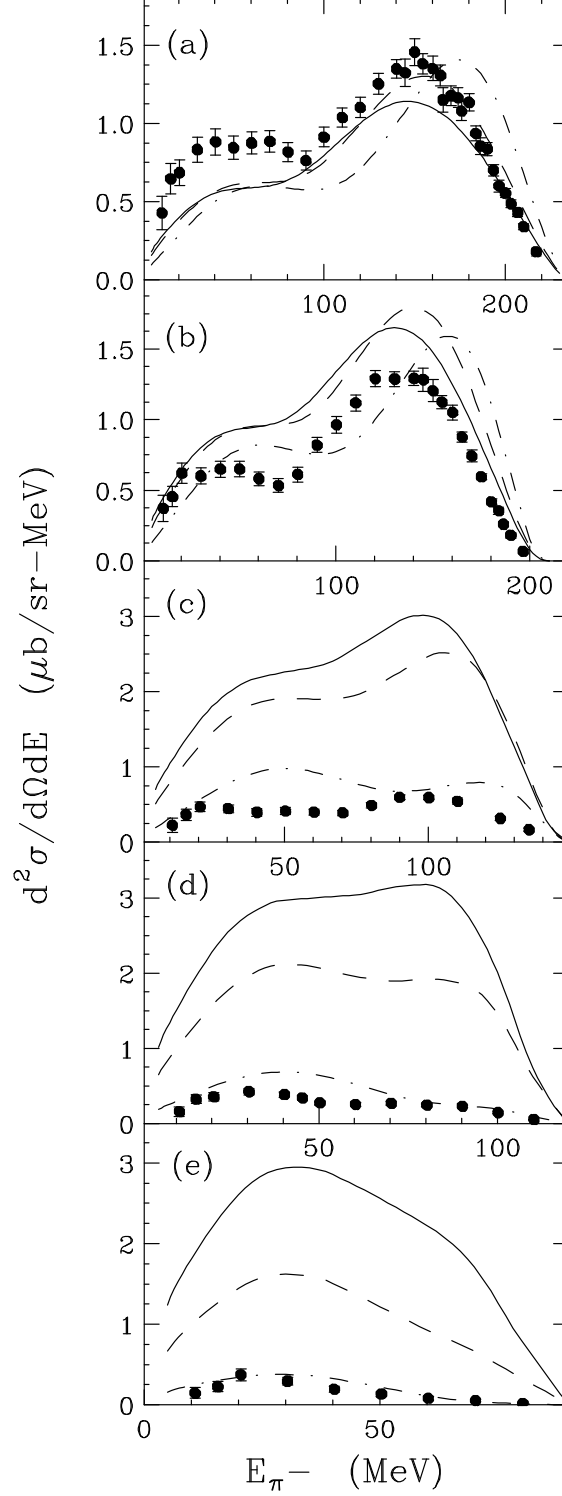


FIG. 21: Doubly differential cross sections for  ${}^4\text{He}(\pi^+, \pi^-)$  at laboratory angle  $25^\circ$  for incident energies 270 (a), 240 (b), 180 (c), 150 (d), and 120 (e) MeV, using the average nuclear potentials  $U_1 = U_2 = -55$  MeV (solid curve),  $U_1 = U_2 = -37$  MeV (dashed curve), and  $U_1 = U_2 = 0$  (dot-dashed curve). The theoretical predictions have not been normalized.

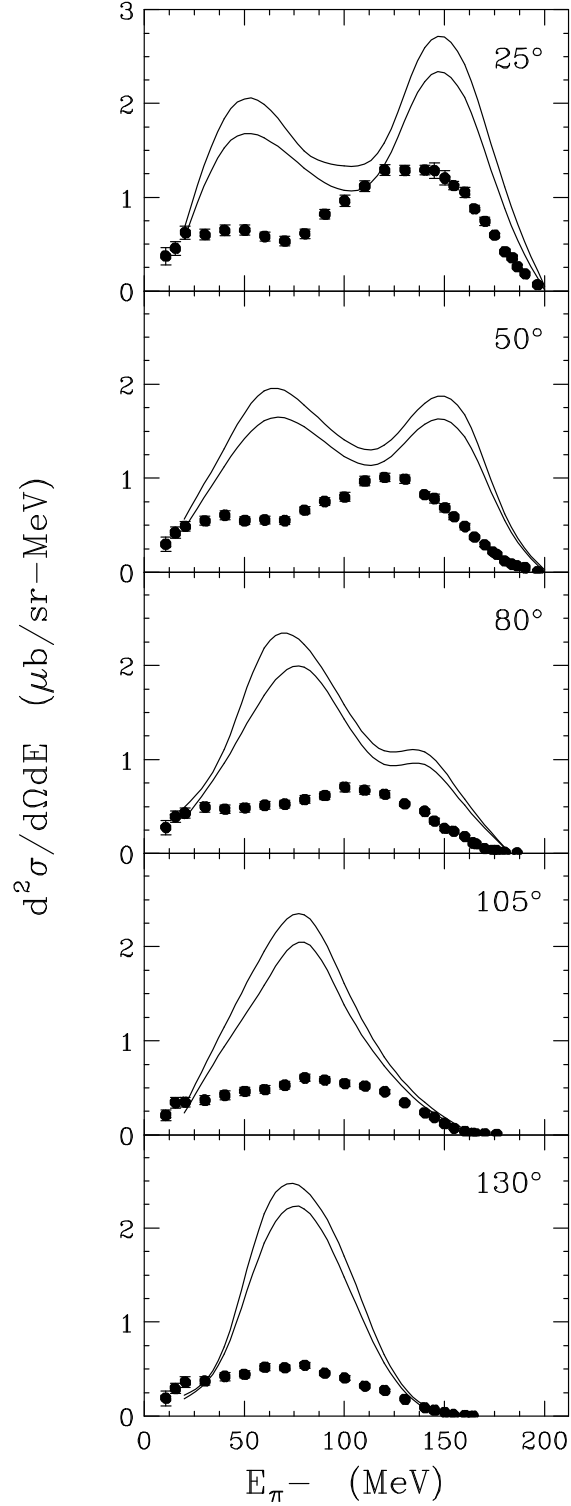


FIG. 22: Comparison of the relativistic three-body model calculation of Kulkarni[38] with the doubly differential cross sections for  ${}^4\text{He}(\pi^+, \pi^-)$  at 240 MeV and laboratory angles  $25^\circ$ ,  $50^\circ$ ,  $80^\circ$ ,  $105^\circ$ , and  $130^\circ$ . The upper and lower curves indicate the uncertainty in the calculation.